JCI The Journal of Clinical Investigation

Inhibition of IRF5 hyper-activation protects from lupus onset and severity

Su Song, … , William L. Clapp, Betsy J. Barnes

J Clin Invest. 2020. https://doi.org/10.1172/JCI120288.

Research In-Press Preview Autoimmunity Immunology

The transcription factor interferon regulatory factor 5 (IRF5) is a central mediator of innate and adaptive immunity. Genetic variations within *IRF5* associate with risk of systemic lupus erythematosus (SLE) and mice lacking*Irf5* are protected from lupus onset and severity, but how IRF5 functions in the context of SLE disease progression remains unclear. Using the NZB/W F1 model of murine lupus, we show that murine Irf5 becomes hyper-activated before clinical onset. In SLE patients, IRF5 hyper-activation correlated with dsDNA titers. To test whether IRF5 hyper-activation is a targetable function, we developed novel inhibitors that are cell permeable, non-toxic and selectively bind to the inactive IRF5 monomer. Preclinical treatment of NZB/W F1 mice with inhibitor attenuated lupus pathology by reducing serum ANA, dsDNA titers and the number of circulating plasma cells, which alleviated kidney pathology and improved survival. Clinical treatment of MRL/lpr and pristane-induced mice with inhibitor led to significant reductions in dsDNA levels and improved survival. In ex vivo human studies, the inhibitor blocked SLE serum-induced IRF5 activation in healthy immune cells and reversed basal IRF5 hyper-activation in SLE immune cells. Altogether, this study provides the first in vivo clinical support for treating SLE patients with an IRF5 inhibitor.

Inhibition of IRF5 hyper-activation protects from lupus onset and severity

Su Song[1†], Saurav De[1,2†‡], Victoria Nelson[1], Samin Chopra[1], Margaret LaPan[1], Kyle Kampta[1], Shan Sun[3], Mingzhu He[3], Cherrie D. Thompson[1], Dan Li[1], Tiffany Shih[1], Natalie Tan[1], Yousef Al-Abed[3], Eugenio Capitle[4], Cynthia Aranow[1], Meggan Mackay[1], William L. Clapp[5], Betsy J. Barnes[1,6*]

[1]Center for Autoimmune Musculoskeletal and Hematopoietic Diseases, Feinstein Institutes for Medical Research, Manhasset, NY 11030

[2]Rutgers Graduate School of Biomedical Sciences, Newark, NJ 07103

[3]Center for Molecular Innovation, Feinstein Institutes for Medical Research, Manhasset, NY 11030

[4]Division of Allergy, Immunology & Rheumatology, Rutgers New Jersey Medical School, Newark, NJ 07103

[5]Department of Pathology, Immunology and Laboratory Medicine, University of Florida, Gainesville, FL 32608

[6]Departments of Molecular Medicine and Pediatrics, Zucker School of Medicine at Hofstra/Northwell, Hempstead, NY 11549

Running Title: Targeting IRF5 hyper-activation alleviates lupus

The authors disclose that B.J.B. is an inventor on patent application US20200071370A1 assigned to Rutgers; B.J.B. and S. Sun are inventors on the U.S. Provisional patent application 50425/733 assigned to Feinstein Institutes.

[†]S. Song and S. De are co-first authors.

[‡]current affiliation is Department of Immunology and Inflammation, Pfizer Inc., Cambridge, MA

[*]Correspondence to: Betsy J. Barnes, The Feinstein Institutes for Medical Research, 350 Community Dr., Manhasset, NY 11030; (tel) 516-562-0434; (email) bbarnes1@northwell.edu

Abstract

The transcription factor interferon regulatory factor 5 (IRF5) is a central mediator of innate and adaptive immunity. Genetic variations within *IRF5* associate with risk of systemic lupus erythematosus (SLE) and mice lacking *Irf5* are protected from lupus onset and severity, but how IRF5 functions in the context of SLE disease progression remains unclear. Using the NZB/W F1 model of murine lupus, we show that murine Irf5 becomes hyper-activated before clinical onset. In SLE patients, IRF5 hyper-activation correlated with dsDNA titers. To test whether IRF5 hyper-activation is a targetable function, we developed inhibitors that are cell permeable, non-toxic and selectively bind to the inactive IRF5 monomer. Preclinical treatment of NZB/W F1 mice with inhibitor attenuated lupus pathology by reducing serum ANA, dsDNA titers and the number of circulating plasma cells (PCs), which alleviated kidney pathology and improved survival. Clinical treatment of MRL/lpr and pristane-induced mice with inhibitor led to significant reductions in dsDNA levels and improved survival. In *ex vivo* human studies, the inhibitor blocked SLE serum-induced IRF5 activation and reversed basal IRF5 hyper-activation in SLE immune cells. Altogether, this study provides the first *in vivo* clinical support for treating SLE patients with an IRF5 inhibitor.

Introduction

Systemic lupus erythematosus (SLE) is a debilitating systemic autoimmune disease characterized by elevated levels of circulating anti-nuclear autoantibodies (ANA) and severe immune dysregulation. Immune dysregulation may be conferred by genetic susceptibility and/or environmental triggers. In the past 50 years, only one new drug has been approved for the treatment of SLE, the monoclonal antibody Belimumab; however, global immunosuppression to control disease activity remains the standard of care. Thus, extensive efforts are underway to develop drugs against targets involved in disease progression. One such new target is interferon regulatory factor 5 (IRF5), a member of the IRF family of transcription factors. IRF5 was originally identified as a regulator of type I interferons (*IFN*s) and IFN-stimulated genes (*ISG*s) in response to virus infection (1-3). Subsequent studies revealed important roles for IRF5 in innate and adaptive immunity, macrophage polarization, cell growth regulation, and apoptosis (4,5). *IRF5* was later identified as an autoimmune susceptibility gene. *IRF5* polymorphisms associate with autoimmune and inflammatory conditions, including inflammatory bowel disease, primary biliary cirrhosis, rheumatoid arthritis, SLE, and systemic sclerosis (6-11). Most well-studied is the role of IRF5 in SLE pathogenesis and a common characteristic amongst SLE patients is increased expression of inflammatory cytokines and type I IFNs that contribute to sustained and persistent autoimmunity (12-17). IRF5 expression is significantly elevated in peripheral blood mononuclear cells (PBMC) from SLE patients as compared to age-matched healthy donors (18), and IRF5 was found to be constitutively activated, *i.e.* nuclear-localized, in SLE monocytes (19). These findings, which implicate IRF5 dysfunction in SLE pathogenesis, are supported by multiple models of murine lupus showing that mice lacking *Irf5* (*Irf5*$^{-/-}$) are protected from disease onset and severity (11,20-26). Equally important and relevant to the therapeutic potential of IRF5 is the finding that lupus

disease is abrogated in *Irf5*$^{+/-}$ mice indicating that a reduction in IRF5 expression and/or activity by only half is sufficient for therapeutic effect (21,24).

Although the mechanism(s) by which IRF5 contributes to disease pathogenesis remains unclear, much of the data point to its role in regulating pro-inflammatory cytokine expression, including IFNα, interleukin (IL) 6, tumor necrosis factor (TNF) α, and IL12, and pathogenic autoantibody production (3,5,11,21-28). Dysregulation of many of these cytokines is associated with disease pathogenesis and IRF5 is predominantly expressed in immune cells (monocytes, dendritic cells and B cells) responsible for their production (29). In an unstimulated cell, IRF5 is localized in the cytoplasm as an inactive monomer (30). While in the inactive conformation, the C-terminal autoinhibitory domain (AID) of IRF5 is thought to either mask the N-terminal DNA binding domain (DBD) and/or the C-terminal protein interaction domain (IAD) that is required for homo/heterodimerization (30,31). Upon activation by post-translational modification events downstream of Toll-like receptors (TLRs), DNA damage, or other antigenic signaling cascades, IRF5 undergoes a conformational change that exposes the IAD for dimerization, and nuclear localization signals (NLS) for translocation (1,30-32). While a significant body of *in vitro* work suggests this conformational shift is dependent on phosphorylation of C-terminal Serine (Ser) residues by activating kinases (33-35), nuclear translocation remains the essential regulatory step mediating IRF5 transcriptional activity (1,30).

Identification of *IRF5* as a global risk factor for autoimmune and inflammatory diseases (5,11,20,36-38), coupled with its increased activation in SLE patient blood, concede IRF5 an attractive target for therapeutic inhibition. While C-terminal phosphorylation and dimerization represent steps amenable to inhibition (39), neither has been definitively shown as an absolute requirement for nuclear translocation (35). An alternate approach to inhibit IRF5 stems from the

finding that either N- or C-terminal regions of IRFs can act as dominant negative (DN) mutants to block transactivation ability (2,29,40-44). Though the mechanism(s) by which DN mutants inhibit IRFs remain unclear, their activity suggests that IRF peptide mimetics may be an effective approach for blocking function. We detail here the *ex vivo* characterization of IRF5 peptide mimetics in healthy and SLE immune cells and *in vivo* characterization in the NZB/W F1, MRL/lpr and pristane-induced models of murine lupus.

Results

IRF5 hyper-activation in SLE patients associates with clinical disease activity

We previously reported elevated IRF5 activation that we refer to here as IRF5 hyper-activation, in SLE Mo from a cohort of SLE patients from Sweden (18). We have extended these original findings in two additional independent cohorts of age- and gender-matched SLE patients and healthy donors from University Hospital in Newark, NJ and Northwell Health in Long Island, NY (**Table 1**). In agreement with previous work, we detected a significant increase in basal IRF5 hyper-activation in SLE Mo ($CD45^+CD14^+$) as compared to healthy donor Mo (**Fig. 1A, Supplemental Fig. 1**). We examined SLE B cells ($CD45^+CD19^+$) and found a similar significant increase (**Fig. 1B**). We attempted to measure IRF5 activation in SLE pDC but were unable to acquire sufficient cellular events for robust statistical analysis (45). We next recruited patients with different stages of clinical disease activity, which led to the finding of a stage-dependent increase in IRF5 hyper-activation within Mo and B cells (**Figs. 1C-D**). Disease activity scoring is defined in **Table 1** and in the Methods section. We further stratified patient data by SLEDAI and dsDNA titers to determine whether IRF5 hyper-activation associates with either clinical phenotype as neither alone defines clinically active disease. We found that basal levels of IRF5 activation were significantly higher in Mo from SLE patients with a SLEDAI ≥4 as compared to SLEDAI=0; no significant difference was found when comparing to a SLEDAI >0<4 (**Fig. 1E**). Similarly, IRF5 hyper-activation was significantly elevated in B cells from SLE patients with a SLEDAI ≥4. Although a positive association between IRF5 hyper-activation and increased SLEDAI score was found in both cell types, neither showed a significant correlation (B cells, r^2=0.03 p=0.32; Mo, r^2=0.08 p=0.07; **Supplemental Fig. 2A-B**). Instead, we found a significant correlation between IRF5 hyper-activation in SLE B cells or Mo and dsDNA titers (**Fig. 1F-H**). In addition, IRF5

hyper-activation in SLE B cells and Mo was significantly correlated (**Fig. 1I**). Given that IRF5 expression and activation have been previously implicated in a type I IFN gene signature in SLE patients (5,11,19-20, 46), we examined whether IRF5 hyper-activation in either cell type correlated with serum IFN-α levels. Somewhat surprising, we detected a significant positive correlation between IRF5 activation in SLE B cells and IFN-α levels but not in SLE Mo (**Fig. 1J-K**). No significant correlation was found between dsDNA and SLEDAI or either with IFN-α levels (**Supplemental Fig. 2C-E**). Together, data support that IRF5 hyper-activation may be a systemic marker of disease activity and severity.

Irf5 is hyper-activated in Mo and B cells from NZB/W F1 mice

Irf5$^{-/-}$ mice have been examined in numerous models of murine lupus with all reports showing that loss of *Irf5* protects mice from disease onset and severity (21-26,47). What is lacking from these studies, though, is an understanding of how Irf5 drives lupus pathogenesis, which is relevant to human SLE. Here, we used the NZB/W F1 model of murine lupus to characterize changes in Irf5 activation by imaging flow cytometry in immune cell subsets before and during clinical onset (**Supplemental Fig. 3A**). NZB/W F1 is a classic, spontaneous model that develops severe lupus-like phenotypes comparable to SLE patients (48). Disease onset and severity can be heterogeneous between mice, yet clinical onset generally occurs ~19-21 weeks-old when proteinuria levels begin to increase and dsDNA antibodies are detectable. Somewhat surprising, we detected dramatic increases in basal Irf5 activation in CD11b^{+} Mo and B220^{+} B cells during early clinical onset, as early as ~10 weeks-old (**Fig. 1L-Q**). This increase was not detected in CD4^{+} or CD8^{+} T cells (**Fig. 1R-S**), nor was it detected in any immune cell subset from age- and gender-matched wild-type Balb/c or C57Bl/6 mice (**Fig. 1L-S** and data not shown). Further, Irf5 expression remained

relatively unchanged over the course of disease (**Supplemental Fig. 3B-C**). These data support that Irf5 hyper-activation may be a driver of murine lupus onset in NZB/W F1 mice.

Design of peptide mimetics that specifically bind to IRF5

Given the distinct findings of IRF5 hyper-activation in immune cells from SLE patients and NZB/W F1 lupus mice, we designed a series of inhibitors that would potentially bind to and inhibit IRF5 activation. We used data from IRF crystal structures and IRF5 DN mutants (2,29,31,40) to generate a series of peptide mimetics that correspond to the N-terminus of IRF5 and might stabilize or maintain the inactive IRF5 monomer, thus inhibiting IRF5 nuclear translocation. Since a crystal structure containing the IRF5 N-terminus has yet to be resolved (31), and the DBD of IRFs is highly homologous, we used coordinates from the resolved IRF3 DBD to build an N-terminal homology model of IRF5 (49). This model was used to predict amino acid sequences with different characteristics that may lead to interaction with the IRF5 C-terminus. Sequence predictions were based on solvent accessible surface, charge, and hydrophobicity (**Fig. 2A-B**, **Supplemental Table 1**). In order for the peptides to transduce the cell membrane, IRF5 sequences were combined with a protein transduction domain (PTD). The PTD has been previously shown to facilitate cell permeability of small peptides (50).

Peptides (1 μM) were tested for their ability to directly interact with human full-length recombinant IRF5 variant 5 (isoform V5) by surface plasmon resonance (SPR) analysis. DWEYS peptide served as a non-targeted control and PTD as a control for the cell permeable sequence. DWEYS showed no affinity for IRF5 and PTD had minimal binding affinity (**Fig. 2C**). N5-1 and N5-2 showed the strongest affinity for IRF5, with N5-3 binding to a slightly lesser extent; N5-5 showed no affinity for IRF5 (binding affinity for IRF5: N5-1≥N5-2>N5-3>N5-4>PTD>N5-5). A

shared similarity between N5-1 and N5-2 is their relatively stronger positive charge, as compared to the others (**Supplemental Table 1**).

Human IRF5 contains two nuclear localization signals (NLS), one in the N-terminus and one in the C-terminus (30). N5-1 corresponds to the N-terminal NLS (PRRVRLK). To test whether any NLS is capable of binding to IRF5, we generated C5-2 that corresponds to the C-terminal NLS (PREKKLI) and examined binding by SPR. C5-2 and PTD bound with similar low affinities (**Fig. 2C**). We have thus identified first generation peptide mimetics (N5-1, N5-2 and N5-3) that directly bind to the full-length inactive IRF5 monomer. The observed difference in function between N5-1 and C5-2 supports that the NLS is not the driver of inhibitor activity and instead, peptide mimetics showing the strongest binding affinity for IRF5 (N5-1, N5-2) are those positively charged and relatively surface accessible.

Peptide mimetics inhibit TLR7-induced IRF5 nuclear translocation

We next sought to determine whether *in vitro* binding data would translate into IRF5 cellular inhibition. IRF5 is a key downstream mediator of TLR7-induced cytokine expression and TLR7 signaling has been implicated in SLE pathogenesis (2,51-54). We examined the ability of IRF5 peptide mimetics to inhibit IRF5 nuclear translocation following stimulation of PBMC with R848. We focused on peptides that showed binding to IRF5 by SPR and included PTD and C5-2 as negative controls. For the initial screening, isolated PBMC from healthy donors were pre-incubated in the presence of mock (PBS), or 10 μM PTD, N5-1, N5-2, N5-3 or C5-2 inhibitor for 1 h followed by stimulation with 500 ng/mL of R848 for 2 h. Cells were surface-stained with anti-CD14 (Mo) and anti-CD19 (B cells) antibodies, then permeabilized and stained for intracellular IRF5 and DRAQ5. R848 induced significant IRF5 nuclear translocation in mock-incubated Mo

(2) (**Fig. 2D**) and B cells (**Fig. 2E**). While pre-incubation with PTD had no significant effect on R848-induced IRF5 nuclear translocation in either cell type, N5-1, N5-2 and N5-3 provided a significant reduction in R848-induced nuclear translocation in Mo (**Fig. 2D**). In B cells, only N5-1 gave a significant reduction in R848-induced IRF5 nuclear translocation (**Fig. 2E**). Surprisingly, pre-incubation with C5-2 showed some reduction in nuclear-localized IRF5 even though there was low binding affinity (**Fig. 2C**); inhibition failed to achieve statistical significance. In unstimulated cells, it is noteworthy that N5-1 and C5-2 had no effect on baseline levels of nuclear-localized IRF5 (grey bars), while N5-2 and N5-3 gave increased basal IRF5 nuclear translocation (**Fig. 2D-E**). Since N5-1 provided potent inhibition in both cell types, we determined the equilibrium dissociation constant (K_D) for N5-1 binding to IRF5 (**Fig. 2F**). A K_D=98.8 nM was calculated supporting a strong binding affinity between N5-1 and the inactive full-length IRF5 monomer that is in agreement with functional data (**Fig. 2D-E**). To further confirm SPR data and analyze inhibitor specificity, we developed an in-cell FRET assay to measure binding of inhibitors to endogenous IRF5, as well as other IRF family members with similar structural and functional domains - IRF3 and IRF7. We only obtained a positive FRET signal for N5-1 binding to endogenous IRF5 and not IRF3 or IRF7 in human primary Mo (**Fig. 2G**). We also tested if PTD that is positively charged like N5-1, and C5-2 that has a neutral charge, could bind to the IRFs. We were unable to detect binding of PTD or C5-2 to any IRF supporting that N5-1 specificity is more related to the peptide sequence than the positive charge. Last, we performed acceptor photobleaching FRET as a secondary, independent method of confirmation and found that N5-1 specifically binds to IRF5 and not IRF3 or IRF7 (**Fig. 2H-L**, **Supplemental Fig. 4A-C**). Together, these findings support the specificity of N5-1 for IRF5.

N5-1 binds to and stabilizes the inactive IRF5 monomer

To gain insight into N5-1 binding to IRF5 at the atomic level, we applied molecular modeling studies. We reasoned that N5-1 must interact with monomeric IRF5 at the IAD in the cytoplasm of a cell rather than the DBD since data from both SPR analysis and in-cell FRET assays indicated direct binding of N5-1 to the inactive full-length IRF5 monomer. To test this, we generated a homology model of inactive IRF5 C-terminal domain using the monomeric autoinhibited IRF3 C-terminal domain (PDB: 1QWT) (49) as a template. The model showed good overall alignment with the α-carbon backbone of the template with an RMSD less than 0.7Å. N5-1 was then docked to IRF5 and ranked by molecular mechanics generalized born surface area (MM-GBSA) binding free energy ($\Delta G_{binding}$) (**Supplemental Table 2**, **Supplemental Fig. 4D**). The top ranked N5-1 peptide-docked pose with a $\Delta G_{binding}$ value of -111.087 kcal/mol is shown in **Fig. 3A**. Meanwhile, C5-2 was docked to the same model as a reference and no pose was predicted. These data provide further support for the select binding of N5-1 to IRF5.

We identified three arginine residues within N5-1 that formed stable hydrogen bonds and salt bridges with the acidic amino acids Asp449, Glu251 and Glu428 on IRF5 (**Fig. 3A**). These amino acids are located on the AID folded loop, the AID helix bundle 4 and the β-sandwich region on the IAD, respectively. Therefore, N5-1 binds to IRF5 and anchors the flexible AID loop onto the IAD. Since activation of IRF5 requires phosphorylation on the Ser-rich region (SRR) to generate the charge repulsion force to destabilize the inactive folded conformation of the AID, we proposed that stabilization of the AID loop in a folded conformation near helix 4 will mask C-terminal IRF5 phosphorylation sites (30,31,33-35). Others and we previously identified key C-terminal Ser residues critical for IRF5 activation, yet antibodies to detect these residues are unavailable (30,31,35). Subsequent studies identified IKK-β as a kinase that phosphorylates

human IRF5 at Ser462 in response to TLR stimulation (33,34). In an effort to develop experimental data that would prove or disprove this binding model, we examined IRF5 phosphorylation at Ser462 (pIRF5). PBMC were stimulated with R848 and IRF5 phosphorylation detected with pIRF5 antibodies (34). Elevated pIRF5 levels were detected in R848-stimulated cells and pre-incubation with N5-1 significantly reduced levels down to mock (**Fig. 3B**). These data provide the initial mechanistic support that N5-1 binds to a region that stabilizes the inactive IRF5 monomer in a conformation that inhibits phosphorylation at Ser462.

Since the N5-1 sequence was extracted from the IRF5 DBD, we projected that the DBD folds onto the C-terminal IAD (**Fig. 3C**). Molecular modeling indicates that this occurs without much steric hindrance. Thus, we propose that in unstimulated cells, the N-terminal DBD is folded over the C-terminal IAD in the full-length inactive IRF5 monomer (**Fig. 3C, left**). The N5-1 sequence within the DBD offers electrostatic interactions to stabilize the folded conformation of the AID loop, which masks the critical phosphorylation sites. Meanwhile, the DBD α3 helix, which contains all of the conserved residues and is responsible for protein-DNA contacts (55,56), is shielded in this position. Upon phosphorylation, the large charge repulsion force on the SRR causes the dramatic conformational change to unfold the AID loop which frees helix 5 for dimerization (**Fig. 3C, right**). It has been observed in the IRF3 crystal structure that the N-terminal region of the IAD undergoes large conformational changes during activation (55,57). Since the DBD links to the N-terminus of the IAD, we predict that the DBD can be released from this folded, inactive position and be exposed to DNA for binding after the confomational change (56) (**Fig. 3C**).

IRF5 peptide mimetics readily enter cells and have low associated toxicity

Next, we synthesized peptides conjugated to FITC (**Supplemental Table 1**) to measure cellular uptake by flow cytometry. Isolated PBMCs were treated with FITC-conjugated PTD, N5-1 or C5-2 for 1 h, and surface-stained to identify Mo and B cells. Representative histogram plots in **Fig. 4A** show increased FITC intensity from PTD and N5-1 in Mo and B cells. Similar findings were made for C5-2 (data not shown). Summarized data from multiple independent donors over a dose range revealed the preferential uptake of N5-1 into Mo rather than B cells (**Fig. 4B**). However, unlike Mo that showed similar uptake of N5-1 over the range, uptake into B cells was dose-dependent (**Fig. 4B**). To confirm that FITC-conjugated inhibitors enter cells and do not simply bind to the surface upon pre-incubation, cell uptake was examined using imaging flow cytometry. At 10 μM, we show that multiple cell types – Mo, B cells and pDC - take up the inhibitors efficiently, as determined by co-staining with nuclear DRAQ5 (**Fig. 4C**). Inhibitor toxicity was assessed by staining PBMCs with propidium iodide or tryphan blue after treatment; minimal toxicity was found (**Supplemental Fig. 5A-B**). IRF5 has been previously shown to regulate cell cycle and apoptosis (58). We examined cell cycle progression as a potential off-target effect of the inhibitors and found no significant difference (**Supplemental Fig. 5C**). No significant change in cellular apoptosis was detected by Annexin V-Sytox co-staining (**Supplemental Fig. 5D**). Together, these data confirm that IRF5 inhibitors enter the cell, are non-toxic, and have limited off-target effects. They also suggest that cell type-specificity may be achieved through varied inhibitor dosing.

N5-1 is a potent inhibitor of TLR7-induced IRF5 nuclear translocation in Mo and B cells

To confirm a block in IRF5 nuclear translocation by the inhibitors, we performed imaging flow cytometry and cell fractionation. PBMC from healthy donors were pre-treated with 10 μM PTD,

N5-1 or C5-2 prior to R848 stimulation. Representative images from mock pre-incubated and unstimulated (NT) PBMC show cytoplasmic IRF5 staining as a green halo around the DRAQ5-positive nucleus in both Mo and B cells (**Fig. 4D**). Upon stimulation, IRF5 translocates to the nucleus, which is shown by the yellow nuclear co-stain. Pre-incubation with inhibitors followed by stimulation resulted in a significant reduction of nuclear IRF5 by N5-1 (**Fig. 4E-F**). Additionally, cell fractionation was performed on isolated primary Mo that were pre-treated with 2.5 μM inhibitor and then stimulated with R848 for 2 h. Western blot analysis of nuclear lysates confirmed imaging flow data showing a marked decrease in R848-induced IRF5 nuclear translocation by N5-1 (**Fig. 4G-H**). We next quantified IRF5 expression in Mo from imaging flow data to determine whether inhibitors alter expression. While no change in basal IRF5 protein expression was detected in NT Mo pre-incubated with inhibitor, the observed upregulation of IRF5 by R848 was not seen in cells pre-incubated with N5-1 (**Supplemental Fig. 6A**).

N5-1 selectively inhibits IRF5-mediated inflammatory cytokine expression

Following IRF5 phosphorylation, homo-dimerization and nuclear translocation, IRF5 binds to the promoters of target genes and regulates their expression (1,3,59). In SLE it is thought that increased levels of pro-inflammatory cytokines contribute to systemic inflammation (12,13). We thus determined whether inhibition of IRF5 nuclear translocation would reduce inflammatory cytokine expression. PBMC were pre-treated with 10 μM inhibitor, stimulated with R848 for 2 h, and total RNA isolated to determine *IL6* and *IFNA* expression by qRT-PCR. Expression of both cytokines was significantly reduced by N5-1 (**Supplemental Fig. 6B-C**). No significant difference was found with PTD or C5-2. Since other transcription factors, such as NF-κB and IRF7, undergo nuclear translocation in response to TLR signaling that results in similar pro-inflammatory

cytokine expression (60,61), we examined the effect of N5-1 on R848-induced NF-κB nuclear translocation in Mo and CpG-A (TLR9)-induced IRF7 nuclear translocation in pDCs. Importantly, the kinetics of NF-κB nuclear translocation are distinct from IRF5. In R848-stimulated Mo, NF-κB nuclear translocation is more rapid and is not detected at 2 h. Instead, the effect of N5-1 on NF-κB nuclear translocation was tested in PBMC after 1 h pre-incubation with inhibitor and stimulation with R848 for 30 min. As expected, R848 induced significant accumulation of nuclear NF-κB (**Supplemental Fig. 6D**), while inhibitors had no significant effect on basal or R848-induced nuclear NF-κB. Similar results were obtained for IRF7 in pDCs after stimulation with CpG-A for 2 h (**Supplemental Fig. 6E**). These data support that N5-1 reduces pro-inflammatory cytokine expression through the select inhibition of IRF5 activation.

N5-1 protects NZB/W F1 mice from spontaneous lupus onset

To test whether Irf5 hyper-activation is a driver of lupus onset and severity in NZB/W F1 mice, we determined whether N5-1 could inhibit murine Irf5 nuclear translocation. RAW264.7 macrophages were pre-incubated with N5-1, stimulated with LPS or R848 for 2 h, and then nuclear extracts isolated for Western blot analysis. Similar to findings in human Mo (**Fig. 4G-H**), N5-1 provided a significant dose-dependent reduction in Irf5 nuclear translocation (**Fig. 5A-B, Supplemental Fig. 7**). We next examined the ability of FITC-conjugated inhibitors to be taken up *in vivo*. NZB/W F1 mice were injected with inhibitor and uptake monitored by imaging flow cytometry over 2 h. Similar to that found in human PBMC (**Fig. 4B-C**), cell type-specific differences were detected, yet all cells showed uptake of inhibitors (**Supplemental Fig. 8**). Since it is well-established that *Irf5*$^{-/-}$ mice are impaired in their production of IL6 (3,47), we used this model to test the ability of N5-1 to inhibit IL6 production *in vivo*. To confirm *in vivo* specificity,

we compared IL6 production in *Irf5*$^{+/+}$, *Irf5*$^{+/-}$ and *Irf5*$^{-/-}$ littermate mice treated with N5-1 and injected with R848. As expected, R848 induced IL6 production in *Irf5*$^{+/+}$ mice while *Irf5*$^{+/-}$ mice showed attenuated production and *Irf5*$^{-/-}$ mice showed a significant reduction in IL6 (3,62) (**Fig. 5C**). N5-1 treated *Irf5*$^{+/+}$ mice mimicked the level of IL6 produced in R848-injected *Irf5*$^{-/-}$ mice, and no further effect of N5-1 was seen in *Irf5*$^{-/-}$ mice. Last, *Irf5*$^{+/+}$ mice treated with PTD or C5-2 had no significant effect on R848-induced IL6 production. Altogether, these data support the specific inhibition of murine Irf5 function *in vivo* by N5-1.

Based on the observed peak of Irf5 hyper-activation in NZB/W F1 mice (**Fig. 1N,Q**), we developed a pilot dosing regimen to test the effects of N5-1 on lupus disease onset in female mice (**Fig. 5D**). Mice received 5 equal doses of 100 μg N5-1 or equal volume of vehicle control from 8-10 weeks of age and proteinuria was measured weekly to track onset. At 20 weeks-old, proteinuria levels began to significantly drop in N5-1-treated mice (**Supplemental Fig. 9A**) and sera dsDNA autoantibodies were significantly reduced (**Fig. 5E**). Measurement of sera anti-nuclear IgG antibodies (ANA) by HEp-2 ANA at 27 weeks-old revealed a significant reduction by N5-1 (**Fig. 5F-G**). Given recent work implicating IRF5 in human PC differentiation (63), accumulation of age-or autoimmune-associated B cells (ABCs) (27) and antibody secretion, we examined cells in the blood of PBS- and N5-1-treated mice. As expected, the percentage of circulating PCs and ABCs increased with disease severity (64) (**Fig. 5H-I**), even though the total number of B220^{+} B cells remained fairly unchanged (**Supplemental Fig. 9B**). While the percentage of PCs increased significantly during later stages of disease development in PBS-treated mice, no significant change was found in N5-1 treated mice over the course of disease; however, N5-1 significantly reduced the accumulation of PCs at >35 weeks-old (**Fig. 5H, Supplemental Fig. 9C**). Conversely, the percentage of circulating ABCs was found to

significantly increase in both PBS- and N5-1 treated mice, however, N5-1 provided a significant reduction in ABCs at 35 weeks-old (**Fig. 5I, Supplemental Fig. 9C**).

N5-1 attenuates Irf5 hyper-activation in NZB/W F1 mice

The kinetics of Irf5 hyper-activation in Mo and B cells from N5-1-treated NZB/W F1 mice were next monitored. At the observed peak in Irf5 hyper-activation, between ~10-19 weeks-old for both Mo and B cells (**Fig. 1N&Q**), a significant reduction in Irf5 nuclear translocation was detected in N5-1-treated mice (**Fig. 5J-K**). No effect on Irf5 expression was found (**Supplemental Fig. 9D-E**). These data confirm the *in vivo* efficacy of N5-1 in reducing Irf5 hyper-activation.

Reduced kidney pathology and increased overall survival

Survival of a cohort of NZB/W F1 mice was monitored until 40 weeks-old revealing significant protection of N5-1-treated mice from lupus-induced mortality (**Fig. 6A**). Histologic analysis of kidneys revealed amelioration of several parameters of renal injury in N5-1-treated mice, including expansion of the mesangial matrix, presence of hyaline deposits, decreased capillary loops, presence of cellular/fibrocellular crescents, tubular necrosis and deposition of immunocomplexes (**Fig. 6B-G**). In N5-1-treated mice, albumin/creatinine ratios began trending down after 27 weeks (**Supplemental Fig. 9F**) and serum creatinine levels were significantly reduced by 40 weeks-old (**Fig. 6H**). No significant change in body weight between groups was found (**Supplemental Fig. 9G**). Last, we monitored IFNα levels over the course of disease and found that low levels were detectable around 17 weeks of age (65-68), which occurred after or concurrent with IRF5 activation (**Supplemental Fig. 9H**). Unfortunately, IFNα levels were too low to detect significant

differences between groups (data now shown). These data support the *in vivo* utility of N5-1 in protecting NZB/W F1 mice from spontaneous lupus onset and mortality.

N5-1 provides therapeutic efficacy in NZB/W F1, MRL/lpr and pristane-induced lupus mice

We next examined whether N5-1 would increase survival of NZB/W F1 mice in a therapeutic efficacy model where mice already have clinically elevated dsDNA titers, positive ANA, elevated proteinuria and kidney disease (https://www.jax.org/jax-mice-and-services/in-vivo-pharmacology/immunology-services/autoimmune-diseases/lupus-studies). We initiated the 2-week N5-1 dosing regimen in a cohort of 27 week-old NZB/W F1 mice. At this later stage of clinical disease, we detected a modest increase in survival that did not reach statistical significance (**Fig. 7A**). Given the slow onset of lupus in NZB/W F1 mice, we switched to MRL/lpr and pristane-induced mice to further examine N5-1 clinical efficacy. Dosing in MRL/lpr mice was initiated at 8 weeks-old and after confirmation of ANA IgG positivity (**Fig. 7B-C**). ANA, anti-dsDNA antibody titers, proteinuria, IRF5 cellular activation and survival were monitored. As early as 10-weeks old, we detected significant reductions in dsDNA titers in N5-1-treated mice that maintained over the course of disease and contributed to increased survival; significant reductions in proteinuria occurred at 30 weeks (**Fig. 7C-G**, **Supplemental Fig. 10A**). The observed reduction in dsDNA titers corresponded to a significant, concomitant reduction in $B220^+$ Irf5 activation (**Fig. 7H**). Unlike NZB/W F1 mice, however, that showed an early single peak in Irf5 activation (**Fig. 1L-Q**), at least two peaks in Irf5 B cell and Mo activation were detected that continued to increase with age/disease severity (**Fig. 7H, Supplemental Fig. 11A**). Significant, albeit small, reductions in Irf5 activation were detected in Mo and $CD8^+$ T cells of N5-1-treated mice (**Supplemental Fig. 11A-C**). These data suggest that Irf5 activity in MRL/lpr mice more closely mirrors SLE patients

where increased Irf5 activation associated with clinical disease activity and dsDNA titers (**Fig. 1C-D, F-H**).

To further confirm the clinical utility of N5-1, we injected Balb/c mice with pristane (21,47) and treated with N5-1 after ANA detection (**Fig. 7I**). Similar to NZB/W F1 and MRL/lpr mice, we detected significant reductions in dsDNA titers that corresponded to a significant increase in overall survival (**Fig. 7J-L, Supplemental Fig. 10B**). Altogether, these data support that independent of the mechanism of lupus onset (NZB/W F1, MRL/lpr, pristane-induced), N5-1 provided significant clinical benefit at later stages of disease development, which holds tremendous promise for patients with SLE.

N5-1 inhibits SLE serum-induced IRF5 activation and reverses IRF5 hyper-activation in SLE immune cells

Herein, we report for the first time that Irf5 is hyper-activated in immune cells from NZB/W F1 and MRL/lpr lupus prone mice before and during clinical onset, respectively. SLE patients present with elevated basal IRF5 activation that is further increased during active flares (**Fig. 1A-D**). Since the mechanism(s) by which IRF5 becomes activated in SLE patients and murine models of lupus is not yet known and is likely mediated by multiple triggers and pathways (19,30-35), we evaluated N5-1 effects *ex vivo* in response to SLE serum, which is a more complex and disease-relevant trigger of IRF5 activation than pure TLR ligands (19). Healthy donor PBMCs were pre-incubated with inhibitor, stimulated with SLE sera for 2 h, and then IRF5 activation determined (19). N5-1 provided a significant reduction in SLE serum-induced IRF5 activation in pDCs, Mo, and B cells (**Fig. 8A-C**) supporting that N5-1 works in the context of a human SLE-like environment. We next asked whether SLE serum-induced IRF5 activation in healthy donors correlated with IRF5

activation in SLE Mo and B cells from matched patients. Indeed, we found a significant correlation between *ex vivo* and *in vivo* IRF5 activation (**Fig. 8D-E**). Last, we examined whether N5-1 could reverse IRF5 hyper-activation in Mo and B cells from active SLE patients. To our surprise, treatment of SLE PBMC with N5-1 for 1 h provided a significant reduction in basal IRF5 hyper-activation (**Fig. 8F**). These data support the use of N5-1 to treat patients with SLE at different stages of disease development.

Discussion

IRF5 genetic variants that associate with SLE risk were originally identified in 2005 (6) and only recently are studies beginning to shed light on how *IRF5* genetic risk contributes to SLE pathogenesis (20,28,69,70). While these studies ensued the multitude of studies in murine lupus models lacking *Irf5*, together, they support genetic and non-genetic roles for Irf5 in lupus disease development (21-26,71). Similar to our recent findings in healthy donor *IRF5* risk carriers (69), herein we demonstrate that dysregulated IRF5 activity, rather than expression, is a driver of SLE disease onset and severity. In NZB/W F1 mice, the observed increase in basal Irf5 hyper-activation occurred in both Mo and B cells, but not T cells, and preceded clinical onset. However, in MRL/lpr mice, Irf5 activation coincided with or occurred after clinical onset and was detected in all cell types examined (**Fig. 7H, Supplemental Fig. 11A-C**). The observed differences in the kinetics of Irf5 activation in these two models of spontaneous murine lupus support distinct mechanisms of lupus onset, yet implicate Irf5 immune cell hyper-activation in both (72). In human SLE, IRF5 hyper-activation in Mo and B cells associated with disease activity and correlated with dsDNA titers.

Baseline increases in murine Irf5 activation were first reported in DCs from *Lyn*-deficient mice suffering from lupus (73). Lyn is a Src family kinase that functions in multiple aspects of immune signaling as both a positive and negative regulator (74,75). Lyn was identified as a negative regulator of IRF5 post-translational modification via direct binding to IRF5 (73). Given that basal IRF5 hyper-activation has been detected in multiple cohorts of lupus patients and more recently in healthy donor *IRF5* genetic risk carriers (69), combined with the finding that Irf5 hyper-activation in NZB/W F1 and MRL/lpr lupus mice was not constitutive over the course of disease, it is unlikely that alterations in *Lyn* are driving IRF5 hyper-activation. Further, since SLE serum

recapitulated IRF5 activation detected in matched SLE patients, this points to a circulating trigger(s) that induces IRF5 activation rather than a loss in negative control regulators (**Fig. 8D-E**) (19). Last, given the heterogeneity of SLE and the differential kinetics and cell type-specificity of Irf5 activation in NZB/W F1 and MRL/lpr mice, it is unlikely that there is a single trigger or pathway leading to IRF5 activation. Indeed, we recently reported that the kinetics of Ser462 IRF5 phosphorylation and nuclear translocation were distinct depending on the stimulus (39). Unfortunately, this phospho-antibody does not detect endogenous IRF5 by Western blot (34), nor were we successful in detecting murine Irf5. Thus, mapping post-translational events on IRF5 in these different model systems would provide valuable insight into mechanisms of activation.

Signalling pathways have emerged as key targets for the development of small molecule inhibitors, with the primary targets being protein kinases and phosphatases (76,77). A caveat to this type of therapeutic targeting is that it requires *a priori* knowledge of the signalling molecules leading to activation. Additionally, kinase inhibitors are often not specific to one kinase, one signaling pathway, nor one downstream target protein. In the case of IRF5, it is well-documented that IRF5 becomes activated in a cell type- and stimuli-dependent manner (1,29,33-35,78-80). Regulation of cytokine production by IRF5 requires nuclear translocation and transcriptional modulation of target genes. Previous work suggested a requirement for ubiquitination and/or acetylation before phosphorylation and homo/hetero-dimerization, which may or may not lead to nuclear translocation (35,81,82). Further, IRF5 phosphorylation occurs at multiple sites that is dependent on the pathway of activation (30-35). Thus, in order to bypass the ambiguity of post-translational modifications and dimerization, we developed peptide mimetics that directly bind to and inhibit IRF5 activation independent of the initiating pathway.

In support of this rationale, we recently characterized another family of cell permeable peptides that inhibit IRF5 dimerization (39). Unfortunately, these inhibitors were not stable for *in vivo* analysis, nor did they similarly inhibit both human and murine IRF5. Targeting IRF5 inhibition in a cell type-specific manner may be feasible as we observed cell type-specificity for N5-1, N5-2 and N5-3 that may be dose-dependent and due to distinct physicochemical properties of each inhibitor (**Figs. 2 & 4**). Although N5-2 and N5-3 were capable of inhibiting R848-induced IRF5 nuclear translocation in Mo, they had little effect on IRF5 in B cells. This may be due to differential binding of N5-2 and N5-3 to IRF5 or differential uptake. Given the high binding affinity of N5-2 and N5-3 for IRF5, data warrant further investigation of these inhibitors. The PTD enables cell permeability, yet endocytosis and macropinocytosis play a role in peptide uptake (50). Thus, differences in both endocytosis and pinocytosis between cell types may account for differences in uptake (**Supplemental Fig. 8**). Additional studies will be required to discern cell type-specific effects of the inhibitors.

Among the most significant outcomes from N5-1 was the finding of long-term protection from spontaneous lupus onset and severity in NZB/W F1 mice treated for only 2 weeks. Sustained effects were observed out to 40 weeks-old. These data suggest that either N5-1 is stable over long periods of time *in vivo* and/or Irf5 hyper-activation is an early, targetable driver of lupus onset. The latter is more likely given the expected shorter half-life of peptide inhibitors; however, we were able to detect a significant reversal in Irf5 hyper-activation in mice between 14-21 weeks-old (**Fig. 5J-K**). Another striking finding was that N5-1 proved clinically efficacious in NZB/W F1, MRL/lpr and pristane-induced lupus mice when given after disease onset (**Fig. 7**). In NZB/W F1 mice, the *in vivo* inhibition of Irf5 hyper-activation by N5-1 resulted in the reversal of several key pathogenic phenotypes that associate with lupus severity, including serum ANA positivity,

elevated dsDNA titers, expansion of circulating PCs and ABCs, and renal injury. Importantly, similar findings of reduced ANA and dsDNA titers, along with increased survival were made in MRL/lpr and pristane-induced mice after clinical treatment. The finding of decreased ANA and dsDNA titers in N5-1-treated NZB/W F1 mice before detection of a significant decrease in PCs and ABCs (**Fig. 5E-I**) is interesting and reminiscent of findings from IRF5 knockdown in human primary B cells showing a larger decrease in secreted IgG isotypes than intracellular isotypes (63). Thus, in addition to playing a role in PC differentiation, these data provide added support that IRF5 may regulate antibody secretion (63). Our finding of *in vivo* IL6 inhibition by N5-1 was also notable as it mimicked IL6 levels seen in R848-injected *Irf5*$^{-/-}$ mice. Further, N5-1 provided no additional effect on IL6 production in *Irf5*$^{-/-}$ mice, supporting the specificity of N5-1 for Irf5. Treatment of healthy donor blood *ex vivo* with N5-1 confirmed the reduction in IRF5-mediated proinflammatory cytokines (*IL6* and *IFNA*). Interestingly, N5-1 had no impact on TLR signaling itself as TLR7- and TLR9-induced NFκB and IRF7 nuclear translocation normally (**Supplemental Fig. 6D-E**). Altogether, these data concede that IRF5 represents a particularly valuable dual function therapeutic target to treat autoimmune and inflammatory diseases. To date, this is the first report of a selective IRF5 inhibitor that directly binds to IRF5 to inhibit nuclear translocation and has *in vivo* clinical efficacy in murine models of lupus (39,83,84).

Methods

Methods can be found in the Supplemental section.

Statistics

Two-tailed Student's *t*-test was used for comparisons between two samples with normal distribution. Prior to test, graph kurtosis was analyzed to ensure normal distribution. For comparisons of one factor over multiple groups, one-way ANOVA was performed followed by Bonferroni's multiple comparisons test. For comparisons of multiple factors over multiple groups, two-way ANOVA was performed followed by Bonferroni's multiple comparisons test. Correlation analysis was performed by linear regression using Pearson's correlation coefficient. Levels of proteinuria and body weight were compared by multiple *t* test, and FDR values were calculated using the Benjamin-Hochberg method to consider false positive associations (threshold of 0.05). Mann-Whitney test was used for ANA-HEp2 and pathologic scoring. Survival curves were derived using the Kaplan-Meier method. GraphPad Prism 6 was used for statistical analysis and graphing. $P < 0.05$ was considered significant. All results from SLE patients and mice were presented as means ± SEM. All other data were presented as means ± SD.

Study Approval

All human work was conducted in accordance with the Institutional Review Boards of Rutgers Biomedical and Health Sciences and the Feinstein Institute for Medical Research. All animal care and experimental procedures were conducted in accordance with the *Guide for the Care and Use of Laboratory Animals* and approved by the Institutional Animal Care and Use Committee of the

Feinstein Institute for Medical Research. Informed consent was obtained from all healthy donors and SLE patients.

Author contributions

B.J.B. and S. Song designed experiments. S. Song, S.D., V.N., M.H., D.L., T.S. and N.T. performed *in vitro* experiments. C.D.T. and K.K. performed FRET assays. S. Song, S.C. and M.L. performed *in vivo* experiments. S. Sun performed modeling and docking analyses. S.D., S. Song, S. Sun, B.J.B. and Y.A-A. wrote the manuscript. E.C., M.M. and C.A. provided SLE patient samples. W.L.C performed pathologic analysis of blinded kidney samples. S. Song is designated first co-author as she performed all long-term *in vivo* experiments and completed the project; S.D. is designated second co-author as he began the project and performed all initial inhibitor studies in human cells. All authors participated in data analysis and preparation of the manuscript.

Acknowledgments

We thank EMD Serono for human pIRF5 antibodies provided by MRCPPU Reagents (https://mrcppureagents.dundee.ac.uk) and L. Persaud, S. Kandasami, and A. Shaw for consenting patients. We thank George M. O'Brien from the Kidney Center at Yale for urine and sera analysis (NIH P30 DK079310). **Funding:** This work was supported by grants from the Lupus Research Alliance, NIAMS AR065959-01, FAMRI 123059 and DoD CDMRP Lupus Research Program LRI170107 to B.J.B., the New Jersey Commission on Cancer Research to S.D., and NIH S10 RR033072-01 to Y.A-A. **Data materials availability:** All data associated with this study are present in the paper or Supplementary Materials.

References

1. Barnes BJ, Moore PA, and Pitha PM. Virus-specific activation of a novel interferon regulatory factor, IRF-5, results in the induction of distinct interferon alpha genes. J Biol Chem. 2001;276(26):23382-90.
2. Schoenemeyer A, Barnes BJ, Mancl ME, Latz E, Goutagny N, Pitha PM, Fitzgerald KA, and Golenbock DT. The interferon regulatory factor, IRF5, is a central mediator of toll-like receptor 7 signaling. J Biol Chem. 2005;280(17):17005-12.
3. Takaoka A, Yanai H, Kondo S, Duncan G, Negishi H, Mizutani T, Kano S, Honda K, Ohba Y, Mak TW, et al. Integral role of IRF-5 in the gene induction programme activated by Toll-like receptors. Nature. 2005;434(7030):243-9.
4. Kaur A, Lee LH, Chow SC, and Fang CM. IRF5-mediated immune responses and its implications in immunological disorders. Int Rev Immunol. 2018;37(5):229-48.
5. Ban T, Sato GR, and Tamura T. Regulation and role of the transcription factor IRF5 in innate immune responses and systemic lupus erythematosus. Int Immunol. 2018;30(11):529-36.
6. Sigurdsson S, Nordmark G, Goring HH, Lindroos K, Wiman AC, Sturfelt G, Jonsen A, Rantapaa-Dahlqvist S, Moller B, Kere J, et al. Polymorphisms in the tyrosine kinase 2 and interferon regulatory factor 5 genes are associated with systemic lupus erythematosus. Am J Hum Genet. 2005;76(3):528-37.
7. Hirschfield GM, Liu X, Han Y, Gorlov IP, Lu Y, Xu C, Lu Y, Chen W, Juran BD, Coltescu C, et al. Variants at IRF5-TNPO3, 17q12-21 and MMEL1 are associated with primary biliary cirrhosis. Nat Genet. 2010;42(8):655-7.
8. Dawidowicz K, Allanore Y, Guedj M, Pierlot C, Bombardieri S, Balsa A, Westhovens R, Barrera P, Alves H, Teixeira VH, et al. The interferon regulatory factor 5 gene confers

susceptibility to rheumatoid arthritis and influences its erosive phenotype. Ann Rheum Dis. 2011;70(1):117-21.

9. Gathungu G, Zhang CK, Zhang W, and Cho JH. A two-marker haplotype in the IRF5 gene is associated with inflammatory bowel disease in a North American cohort. Genes Immun. 2012;13(4):351-5.
10. Saigusa R, Asano Y, Taniguchi T, Yamashita T, Ichimura Y, Takahashi T, Toyama T, Yoshizaki A, Sugawara K, Tsuruta D, et al. Multifaceted contribution of the TLR4-activated IRF5 transcription factor in systemic sclerosis. Proc Natl Acad Sci U S A. 2015;112(49):15136-41.
11. Matta B, Song S, Li D, and Barnes BJ. Interferon regulatory factor signaling in autoimmune disease. Cytokine. 2017;98(15-26.
12. Banchereau J, and Pascual V. Type I interferon in systemic lupus erythematosus and other autoimmune diseases. Immunity. 2006;25(3):383-92.
13. Tackey E, Lipsky PE, and Illei GG. Rationale for interleukin-6 blockade in systemic lupus erythematosus. Lupus. 2004;13(5):339-43.
14. Banchereau R, Hong S, Cantarel B, Baldwin N, Baisch J, Edens M, Cepika AM, Acs P, Turner J, Anguiano E, et al. Personalized Immunomonitoring Uncovers Molecular Networks that Stratify Lupus Patients. Cell. 2016;165(3):551-65.
15. Li QZ, Zhou J, Lian Y, Zhang B, Branch VK, Carr-Johnson F, Karp DR, Mohan C, Wakeland EK, and Olsen NJ. Interferon signature gene expression is correlated with autoantibody profiles in patients with incomplete lupus syndromes. Clin Exp Immunol. 2010;159(3):281-91.
16. Ronnblom L, Eloranta ML, and Alm GV. The type I interferon system in systemic lupus

erythematosus. Arthritis Rheum. 2006;54(2):408-20.

17. Ripley BJ, Goncalves B, Isenberg DA, Latchman DS, and Rahman A. Raised levels of interleukin 6 in systemic lupus erythematosus correlate with anaemia. Ann Rheum Dis. 2005;64(6):849-53.
18. Feng D, Stone RC, Eloranta ML, Sangster-Guity N, Nordmark G, Sigurdsson S, Wang C, Alm G, Syvanen AC, Ronnblom L, et al. Genetic variants and disease-associated factors contribute to enhanced interferon regulatory factor 5 expression in blood cells of patients with systemic lupus erythematosus. Arthritis Rheum. 2010;62(2):562-73.
19. Stone RC, Feng D, Deng J, Singh S, Yang L, Fitzgerald-Bocarsly P, Eloranta ML, Ronnblom L, and Barnes BJ. Interferon regulatory factor 5 activation in monocytes of systemic lupus erythematosus patients is triggered by circulating autoantigens independent of type I interferons. Arthritis Rheum. 2012;64(3):788-98.
20. Barnes BJ. Genetic Versus Non-genetic Drivers of SLE: Implications of IRF5 Dysregulation in Both Roads Leading to SLE. Curr Rheumatol Rep. 2019;21(1):2.
21. F eng D, Yang L, Bi X, Stone RC, Patel P, and Barnes BJ. Irf5-deficient mice are protected from pristane-induced lupus via increased Th2 cytokines and altered IgG class switching. Eur J Immunol. 2012;42(6):1477-87.
22. Xu Y, Lee PY, Li Y, Liu C, Zhuang H, Han S, Nacionales DC, Weinstein J, Mathews CE, Moldawer LL, et al. Pleiotropic IFN-dependent and -independent effects of IRF5 on the pathogenesis of experimental lupus. J Immunol. 2012;188(8):4113-21.
23. Tada Y, Kondo S, Aoki S, Koarada S, Inoue H, Suematsu R, Ohta A, Mak TW, and Nagasawa K. Interferon regulatory factor 5 is critical for the development of lupus in MRL/lpr mice. Arthritis Rheum. 2011;63(3):738-48.

24. Richez C, Yasuda K, Bonegio RG, Watkins AA, Aprahamian T, Busto P, Richards RJ, Liu CL, Cheung R, Utz PJ, et al. IFN regulatory factor 5 is required for disease development in the FcgammaRIIB-/-Yaa and FcgammaRIIB-/- mouse models of systemic lupus erythematosus. J Immunol. 2010;184(2):796-806.
25. Watkins AA, Yasuda K, Wilson GE, Aprahamian T, Xie Y, Maganto-Garcia E, Shukla P, Oberlander L, Laskow B, Menn-Josephy H, et al. IRF5 deficiency ameliorates lupus but promotes atherosclerosis and metabolic dysfunction in a mouse model of lupus-associated atherosclerosis. J Immunol. 2015;194(4):1467-79.
26. Savitsky DA, Yanai H, Tamura T, Taniguchi T, and Honda K. Contribution of IRF5 in B cells to the development of murine SLE-like disease through its transcriptional control of the IgG2a locus. Proc Natl Acad Sci U S A. 2010;107(22):10154-9.
27. Manni M, Gupta S, Ricker E, Chinenov Y, Park SH, Shi M, Pannellini T, Jessberger R, Ivashkiv LB, and Pernis AB. Regulation of age-associated B cells by IRF5 in systemic autoimmunity. Nat Immunol. 2018;19(4):407-19.
28. Hedl M, and Abraham C. IRF5 risk polymorphisms contribute to interindividual variance in pattern recognition receptor-mediated cytokine secretion in human monocyte-derived cells. J Immunol. 2012;188(11):5348-56.
29. Mancl ME, Hu G, Sangster-Guity N, Olshalsky SL, Hoops K, Fitzgerald-Bocarsly P, Pitha PM, Pinder K, and Barnes BJ. Two discrete promoters regulate the alternatively spliced human interferon regulatory factor-5 isoforms. Multiple isoforms with distinct cell type-specific expression, localization, regulation, and function. J Biol Chem. 2005;280(22):21078-90.
30. Barnes BJ, Kellum MJ, Field AE, and Pitha PM. Multiple regulatory domains of IRF-5 control activation, cellular localization, and induction of chemokines that mediate recruitment of T

lymphocytes. Mol Cell Biol. 2002;22(16):5721-40.

31. Chen W, Lam SS, Srinath H, Jiang Z, Correia JJ, Schiffer CA, Fitzgerald KA, Lin K, and Royer WE, Jr. Insights into interferon regulatory factor activation from the crystal structure of dimeric IRF5. Nat Struct Mol Biol. 2008;15(11):1213-20.
32. Lin R, Yang L, Arguello M, Penafuerte C, and Hiscott J. A CRM1-dependent nuclear export pathway is involved in the regulation of IRF-5 subcellular localization. J Biol Chem. 2005;280(4):3088-95.
33. Ren J, Chen X, and Chen ZJ. IKKbeta is an IRF5 kinase that instigates inflammation. Proc Natl Acad Sci U S A. 2014;111(49):17438-43.
34. Lopez-Pelaez M, Lamont DJ, Peggie M, Shpiro N, Gray NS, and Cohen P. Protein kinase IKKbeta-catalyzed phosphorylation of IRF5 at Ser462 induces its dimerization and nuclear translocation in myeloid cells. Proc Natl Acad Sci U S A. 2014;111(49):17432-7.
35. Chang Foreman HC, Van Scoy S, Cheng TF, and Reich NC. Activation of interferon regulatory factor 5 by site specific phosphorylation. PLoS One. 2012;7(3):e33098.
36. Alzaid F, Lagadec F, Albuquerque M, Ballaire R, Orliaguet L, Hainault I, Blugeon C, Lemoine S, Lehuen A, Saliba DG, et al. IRF5 governs liver macrophage activation that promotes hepatic fibrosis in mice and humans. JCI Insight. 2016;1(20):e88689.
37. Sun K, He SB, Qu JG, Dang SC, Chen JX, Gong AH, Xie R, and Zhang JX. IRF5 regulates lung macrophages M2 polarization during severe acute pancreatitis in vitro. World J Gastroenterol. 2016;22(42):9368-77.
38. Byrne AJ, Weiss M, Mathie SA, Walker SA, Eames HL, Saliba D, Lloyd CM, and Udalova IA. A critical role for IRF5 in regulating allergic airway inflammation. Mucosal Immunol. 2017;10(3):716-26.

39. Banga J, Srinivasan D, Sun CC, Thompson CD, Milletti F, Huang KS, Hamilton S, Song S, Hoffman AF, Qin YG, et al. Inhibition of IRF5 cellular activity with cell-penetrating peptides that target homodimerization. Sci Adv. 2020;6(20):eaay1057.
40. Martin HJ, Lee JM, Walls D, and Hayward SD. Manipulation of the toll-like receptor 7 signaling pathway by Epstein-Barr virus. J Virol. 2007;81(18):9748-58.
41. Yang L, Zhao T, Shi X, Nakhaei P, Wang Y, Sun Q, Hiscott J, and Lin R. Functional analysis of a dominant negative mutation of interferon regulatory factor 5. PLoS One. 2009;4(5):e5500.
42. Ren Z, Wang Y, Tao D, Liebenson D, Liggett T, Goswami R, Clarke R, Stefoski D, and Balabanov R. Overexpression of the dominant-negative form of interferon regulatory factor 1 in oligodendrocytes protects against experimental autoimmune encephalomyelitis. J Neurosci. 2011;31(23):8329-41.
43. Kim TY, Lee KH, Chang S, Chung C, Lee HW, Yim J, and Kim TK. Oncogenic potential of a dominant negative mutant of interferon regulatory factor 3. J Biol Chem. 2003;278(17):15272-8.
44. Ning S, Huye LE, and Pagano JS. Regulation of the transcriptional activity of the IRF7 promoter by a pathway independent of interferon signaling. J Biol Chem. 2005;280(13):12262-70.
45. Liao X, Reihl AM, and Luo XM. Breakdown of Immune Tolerance in Systemic Lupus Erythematosus by Dendritic Cells. J Immunol Res. 2016;2016(6269157).
46. Niewold TB, Kelly JA, Flesch MH, Espinoza LR, Harley JB, and Crow MK. Association of the IRF5 risk haplotype with high serum interferon-alpha activity in systemic lupus erythematosus patients. Arthritis Rheum. 2008;58(8):2481-7.
47. Yang L, Feng D, Bi X, Stone RC, and Barnes BJ. Monocytes from Irf5-/- mice have an intrinsic

defect in their response to pristane-induced lupus. J Immunol. 2012;189(7):3741-50.

48. Theofilopoulos AN, and Dixon FJ. Murine models of systemic lupus erythematosus. Adv Immunol. 1985;37(269-390).
49. Takahasi K, Suzuki NN, Horiuchi M, Mori M, Suhara W, Okabe Y, Fukuhara Y, Terasawa H, Akira S, Fujita T, et al. X-ray crystal structure of IRF-3 and its functional implications. Nat Struct Biol. 2003;10(11):922-7.
50. Lin YZ, Yao SY, Veach RA, Torgerson TR, and Hawiger J. Inhibition of nuclear translocation of transcription factor NF-kappa B by a synthetic peptide containing a cell membrane-permeable motif and nuclear localization sequence. J Biol Chem. 1995;270(24):14255-8.
51. Komatsuda A, Wakui H, Iwamoto K, Ozawa M, Togashi M, Masai R, Maki N, Hatakeyama T, and Sawada K. Up-regulated expression of Toll-like receptors mRNAs in peripheral blood mononuclear cells from patients with systemic lupus erythematosus. Clin Exp Immunol. 2008;152(3):482-7.
52. Lyn-Cook BD, Xie C, Oates J, Treadwell E, Word B, Hammons G, and Wiley K. Increased expression of Toll-like receptors (TLRs) 7 and 9 and other cytokines in systemic lupus erythematosus (SLE) patients: ethnic differences and potential new targets for therapeutic drugs. Mol Immunol. 2014;61(1):38-43.
53. Subramanian S, Tus K, Li QZ, Wang A, Tian XH, Zhou J, Liang C, Bartov G, McDaniel LD, Zhou XJ, et al. A Tlr7 translocation accelerates systemic autoimmunity in murine lupus. Proc Natl Acad Sci U S A. 2006;103(26):9970-5.
54. Pisitkun P, Deane JA, Difilippantonio MJ, Tarasenko T, Satterthwaite AB, and Bolland S. Autoreactive B cell responses to RNA-related antigens due to TLR7 gene duplication. Science. 2006;312(5780):1669-72.

55. Qin BY, Liu C, Lam SS, Srinath H, Delston R, Correia JJ, Derynck R, and Lin K. Crystal structure of IRF-3 reveals mechanism of autoinhibition and virus-induced phosphoactivation. Nat Struct Biol. 2003;10(11):913-21.
56. Panne D, Maniatis T, and Harrison SC. An atomic model of the interferon-beta enhanceosome. Cell. 2007;129(6):1111-23.
57. Qin BY, Liu C, Srinath H, Lam SS, Correia JJ, Derynck R, and Lin K. Crystal structure of IRF-3 in complex with CBP. Structure. 2005;13(9):1269-77.
58. Barnes BJ, Kellum MJ, Pinder KE, Frisancho JA, and Pitha PM. Interferon regulatory factor 5, a novel mediator of cell cycle arrest and cell death. Cancer Res. 2003;63(19):6424-31.
59. Barnes BJ, Richards J, Mancl M, Hanash S, Beretta L, and Pitha PM. Global and distinct targets of IRF-5 and IRF-7 during innate response to viral infection. J Biol Chem. 2004;279(43):45194-207.
60. Medzhitov R, and Horng T. Transcriptional control of the inflammatory response. Nat Rev Immunol. 2009;9(10):692-703.
61. Honda K, Yanai H, Negishi H, Asagiri M, Sato M, Mizutani T, Shimada N, Ohba Y, Takaoka A, Yoshida N, et al. IRF-7 is the master regulator of type-I interferon-dependent immune responses. Nature. 2005;434(7034):772-7.
62. Purtha WE, Swiecki M, Colonna M, Diamond MS, and Bhattacharya D. Spontaneous mutation of the Dock2 gene in Irf5-/- mice complicates interpretation of type I interferon production and antibody responses. Proc Natl Acad Sci U S A. 2012;109(15):E898-904.
63. De S, Zhang B, Shih T, Singh S, Winkler A, Donnelly R, and Barnes BJ. B Cell-Intrinsic Role for IRF5 in TLR9/BCR-Induced Human B Cell Activation, Proliferation, and Plasmablast Differentiation. Front Immunol. 2017;8(1938).

64. Rubtsov AV, Rubtsova K, Fischer A, Meehan RT, Gillis JZ, Kappler JW, and Marrack P. Toll-like receptor 7 (TLR7)-driven accumulation of a novel CD11c(+) B-cell population is important for the development of autoimmunity. Blood. 2011;118(5):1305-15.
65. Zhuang H, Szeto C, Han S, Yang L, and Reeves WH. Animal Models of Interferon Signature Positive Lupus. Front Immunol. 2015;6(291).
66. Liu Z, and Davidson A. IFNalpha Inducible Models of Murine SLE. Front Immunol. 2013;4(306).
67. Leng L, Chen L, Fan J, Greven D, Arjona A, Du X, Austin D, Kashgarian M, Yin Z, Huang XR, et al. A small-molecule macrophage migration inhibitory factor antagonist protects against glomerulonephritis in lupus-prone NZB/NZW F1 and MRL/lpr mice. J Immunol. 2011;186(1):527-38.
68. Mathian A, Weinberg A, Gallegos M, Banchereau J, and Koutouzov S. IFN-alpha induces early lethal lupus in preautoimmune (New Zealand Black x New Zealand White) F1 but not in BALB/c mice. J Immunol. 2005;174(5):2499-506.
69. Li D, Matta B, Song S, Nelson V, Diggins K, Simpfendorfer KR, Gregersen PK, Linsley P, and Barnes BJ. IRF5 genetic risk variants drive myeloid-specific IRF5 hyperactivation and presymptomatic SLE. JCI Insight. 2020;5(2).
70. Calise J, Marquez Renteria S, Gregersen PK, and Diamond B. Lineage-Specific Functionality of an Interferon Regulatory Factor 5 Lupus Risk Haplotype: Lack of B Cell Intrinsic Effects. Front Immunol. 2018;9(996.
71. Barnes BJ. Genetic Versus Non-genetic Drivers of SLE: Implications of IRF5 Dysregulation in Both Roads Leading to SLE. Curr Rheumatol Rep. 2019;21(1):2.
72. Richard ML, and Gilkeson G. Mouse models of lupus: what they tell us and what they don't.

Lupus Sci Med. 2018;5(1):e000199.

73. Ban T, Sato GR, Nishiyama A, Akiyama A, Takasuna M, Umehara M, Suzuki S, Ichino M, Matsunaga S, Kimura A, et al. Lyn Kinase Suppresses the Transcriptional Activity of IRF5 in the TLR-MyD88 Pathway to Restrain the Development of Autoimmunity. Immunity. 2016;45(2):319-32.
74. Scapini P, Pereira S, Zhang H, and Lowell CA. Multiple roles of Lyn kinase in myeloid cell signaling and function. Immunol Rev. 2009;228(1):23-40.
75. Xu Y, Harder KW, Huntington ND, Hibbs ML, and Tarlinton DM. Lyn tyrosine kinase: accentuating the positive and the negative. Immunity. 2005;22(1):9-18.
76. Cohen P. Protein kinases--the major drug targets of the twenty-first century? Nat Rev Drug Discov. 2002;1(4):309-15.
77. Ott PA, and Adams S. Small-molecule protein kinase inhibitors and their effects on the immune system: implications for cancer treatment. Immunotherapy. 2011;3(2):213-27.
78. Cushing L, Winkler A, Jelinsky SA, Lee K, Korver W, Hawtin R, Rao VR, Fleming M, and Lin LL. IRAK4 kinase activity controls Toll-like receptor-induced inflammation through the transcription factor IRF5 in primary human monocytes. J Biol Chem. 2017;292(45):18689-98.
79. Hu G, Mancl ME, and Barnes BJ. Signaling through IFN regulatory factor-5 sensitizes p53-deficient tumors to DNA damage-induced apoptosis and cell death. Cancer Res. 2005;65(16):7403-12.
80. Hu G, and Barnes BJ. IRF-5 is a mediator of the death receptor-induced apoptotic signaling pathway. J Biol Chem. 2009;284(5):2767-77.
81. Balkhi MY, Fitzgerald KA, and Pitha PM. Functional regulation of MyD88-activated interferon regulatory factor 5 by K63-linked polyubiquitination. Mol Cell Biol.

2008;28(24):7296-308.

82. Feng D, Sangster-Guity N, Stone R, Korczeniewska J, Mancl ME, Fitzgerald-Bocarsly P, and Barnes BJ. Differential requirement of histone acetylase and deacetylase activities for IRF5-mediated proinflammatory cytokine expression. J Immunol. 2010;185(10):6003-12.
83. Xu H, Krolikowski JG, Jones DW, Ge ZD, Pagel PS, Pritchard KA, Jr., and Weihrauch D. 4F decreases IRF5 expression and activation in hearts of tight skin mice. PLoS One. 2012;7(12):e52046.
84. Weihrauch D, Krolikowski JG, Jones DW, Zaman T, Bamkole O, Struve J, Pillai S, Pagel PS, Lohr NL, and Pritchard KA, Jr. An IRF5 Decoy Peptide Reduces Myocardial Inflammation and Fibrosis and Improves Endothelial Cell Function in Tight-Skin Mice. PLoS One. 2016;11(4):e0151999.
85. Gladman DD, Ibanez D, and Urowitz MB. Systemic lupus erythematosus disease activity index 2000. J Rheumatol. 2002;29(2):288-91.
86. Doucey MA, Goffin L, Naeher D, Michielin O, Baumgartner P, Guillaume P, Palmer E, and Luescher IF. CD3 delta establishes a functional link between the T cell receptor and CD8. J Biol Chem. 2003;278(5):3257-64.
87. Barbato C, Canu N, Zambrano N, Serafino A, Minopoli G, Ciotti MT, Amadoro G, Russo T, and Calissano P. Interaction of Tau with Fe65 links tau to APP. Neurobiol Dis. 2005;18(2):399-408.
88. Poole E, Strappe P, Mok HP, Hicks R, and Lever AM. HIV-1 Gag-RNA interaction occurs at a perinuclear/centrosomal site; analysis by confocal microscopy and FRET. Traffic. 2005;6(9):741-55.
89. Li D, De S, Li D, Song S, Matta B, and Barnes BJ. Specific detection of interferon regulatory

factor 5 (IRF5): A case of antibody inequality. Sci Rep. 2016;6(31002).

90. Giles BM, Tchepeleva SN, Kachinski JJ, Ruff K, Croker BP, Morel L, and Boackle SA. Augmentation of NZB autoimmune phenotypes by the Sle1c murine lupus susceptibility interval. J Immunol. 2007;178(7):4667-75.

Table 1. Demographics of SLE patient population.

	Total	anti-dsDNA titer, mean	SLEDAI-2K (0-105)[†], mean	Disease Activity Score[*] 0	1	2	3
Sex	n (%)						
Female	38(88)	203.7	5	6(16)	10(26)	7(18)	15(40)
Male	5(12)	396.6	7			1(20)	4(80)
Ethnicity/Race	n (%)						
White	6(14)	110.8	4	1	2	1	2
African-American or Afro-Caribbean	23(53)	216.6	5	2	8	3	10
Hispanic	12(28)	192.0	3	3	3	3	3
Asian	2(5)	337	6	0	1	0	1
Age	range (mean)						
	20-70 (40)						
Treatment	n (%)						
Corticosteroids	24(56)						
Anti-malarials	29(67)						
Immunosuppressives	22(51)						

[†]range of 0-20 for this NY cohort. [*]0: no disease activity, normal complement and dsDNA titer, clinical SLEDAI=0; 1: serologically active, clinically stable disease activity, abnormal complement and/or anti-dsDNA titers, clinical SLEDAI=0; 2: mild disease activity, SLEDAI-2K>0<4; 3: moderate to severe disease activity, SLEDAI-2K ≥4. Clinical SLEDAI-2K refers to components of the SLEDAI-2K exclusive of complement values or anti-dsDNA antibody titers.

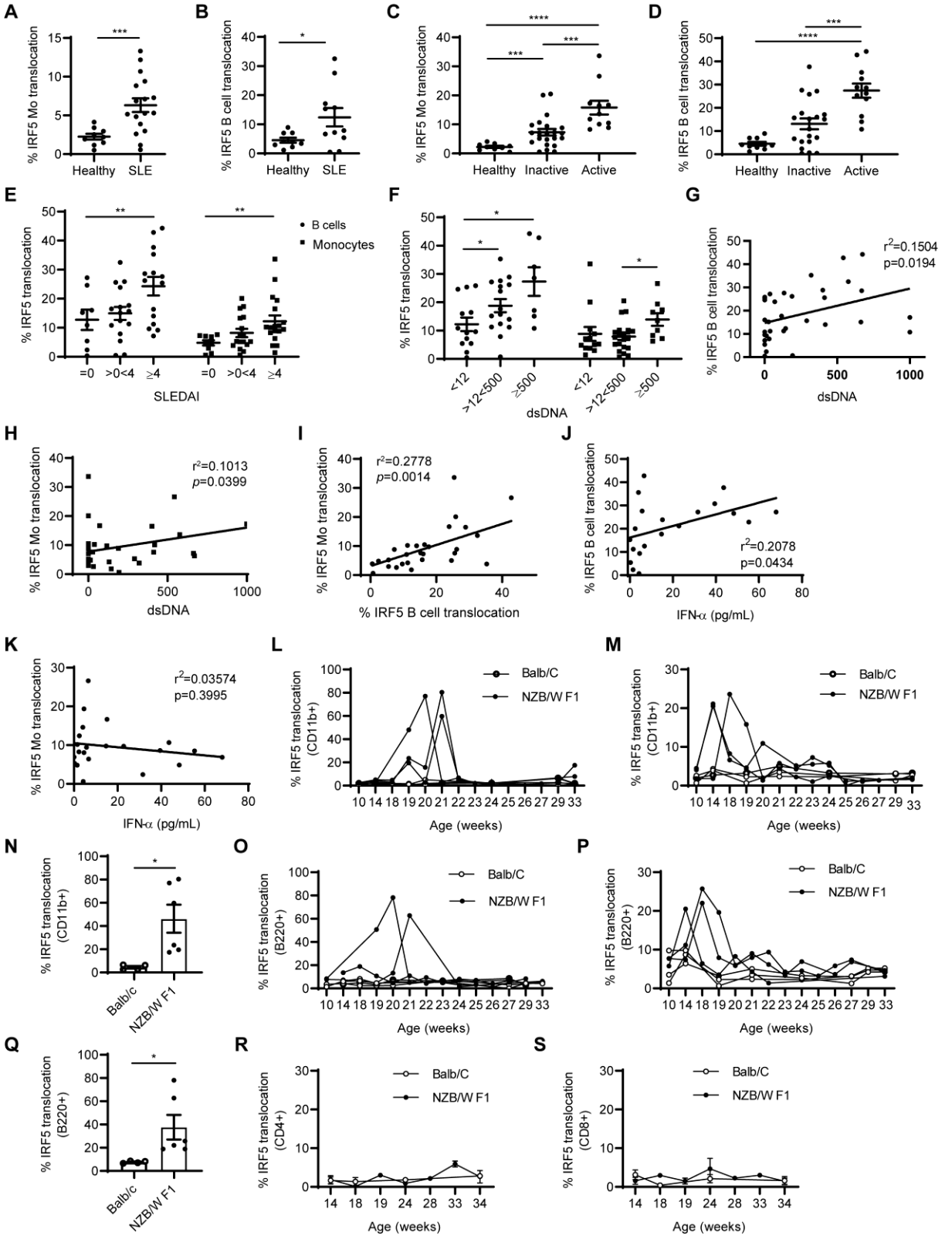

Fig. 1. **IRF5 is hyper-activated in immune cells from SLE patients and NZB/W F1 lupus-prone mice.** IRF5 activation was assessed by nuclear localization in $CD45^{+}CD14^{+}$ Mo (**A**) and

$CD45^+CD19^+$ B cells (**B**) from healthy donors and SLE patients in the NJ cohort using imaging flow cytometry. Data are % IRF5 nuclear translocation; circles represent independent donors. (**C** and **D**) IRF5 localization determined in Mo (**C**) and B cells (**D**) from healthy donors and SLE patients in the NY cohort with clinically inactive (score = 0/1) or active (score 2/3) disease. (**E** and **F**) % IRF5 nuclear translocation in Mo and B cells from SLE patients stratified by SLEDAI (**E**) or dsDNA antibody titer (**F**). (**G-K**) Correlation between % IRF5 translocation in B cells or Mo and dsDNA titers (**G** and **H**) or serum IFNα levels (**J** and **K**) by linear regression analysis. (**L** and **M**) Irf5 nuclear translocation in $CD11b^+$ Mo from cohort 1 (**L**) and cohort 2 (**M**) of aging female NZB/W F1 and Balb/c mice. Black circles-NZB/W F1 mice; open circles-Balb/c. *n* = 3 mice/group/cohort. (**N**) Inhibition of Irf5 activation (10-21weeks-old) by N5-1 in $CD11b^+$ Mo. (**O** and **P**) Same as (**L** and **M**) except in $B220^+$ B cells from cohort 1 (**O**) and cohort 2 (**P**). (**Q**) Same as (**N**) except inhibition of Irf5 activation is shown in $B220^+$ B cells. (**R** and **S**) Irf5 translocation in $CD3^+CD4^+$ T cells (**R**) and $CD3^+CD8^+$ T cells (**S**) from aging female NZB/W F1 and Balb/c mice. *n* = 6 mice/group. Statistical significance was determined using two-way ANOVA with a Bonferroni post hoc test. All values reported as means ± SEM.*($p \leq 0.05$), **($p \leq 0.01$), ***($p \leq 0.001$), ****($p \leq 0.0001$).

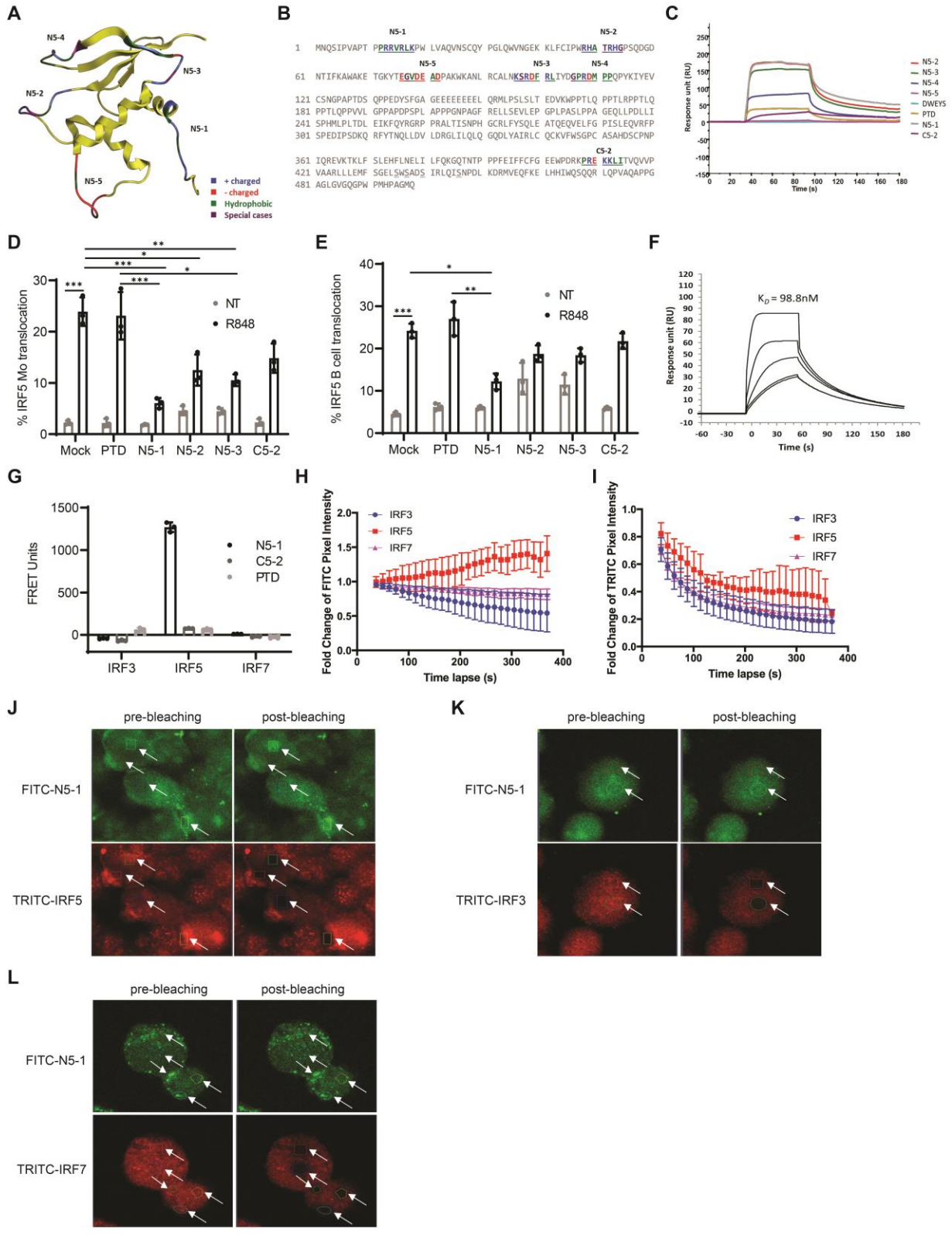

Fig. 2. Design of IRF5 peptide mimetics. (**A**) Homology model of the IRF5 DBD with location of N-terminal peptides and amino acid characteristics. (**B**) Position of N- and C-terminal peptides

highlighted within the full-length IRF5 V5 sequence. Color code is based on amino acid characteristics defined in (**A**). (**C**) Biacore T200 SPR analysis of peptide mimetics. Data are representative of 4 independent experimental replicates per peptide. (**D** and **E**) IRF5 nuclear translocation quantified in healthy donor PBMC pre-incubated with 10 µM peptide for 1 h and stimulated with 500 ng/mL R848 for 2 h using imaging flow cytometry. Quantification in $CD45^+CD14^+$ Mo (**D**) and $CD45^+CD19^+$ B cells (**E**); $n = 3$ independent healthy donors. (**F**) Kinetic analysis of N5-1 peptide binding to IRF5 by SPR. Data are representative of 4 independent experimental replicates. (**G**) Purified human Mo were pre-incubated with either 2.5 µM FITC-PTD, -N5-1 or -C5-2 for 1 h followed by permeabilization and staining for intracellular IRF3, IRF5 or IRF7 with TRITC-conjugated antibodies. FRET units were calculated from fluorescence emissions (see Suppl Methods); n=3 independent healthy donors. (**H-L**) *In vivo* monitoring of the interaction between FITC-N5-1 and endogenous IRF3, IRF5 or IRF7 by acceptor photobleaching FRET microscopy in THP1 cells. (**H** and **I**) Fold-change in donor pixel intensity was monitored in the photobleached regions (**J-L**) and plotted over time. Photobleached regions are denoted by white arrowhead. Images were acquired before and after acceptor photobleaching. Representative images of FITC-N5-1 and TRITC-IRF5 (**J**), TRITC-IRF3 (**K**) or TRITC-IRF7 (**L**) are shown at 60X magnification. Data are representative of 3 independent biological replicates performed in triplicate. Statistical significance was determined by one-way ANOVA. Error bars represent SD. *($p \leq 0.05$), **($p \leq 0.01$), ***($p \leq 0.001$).

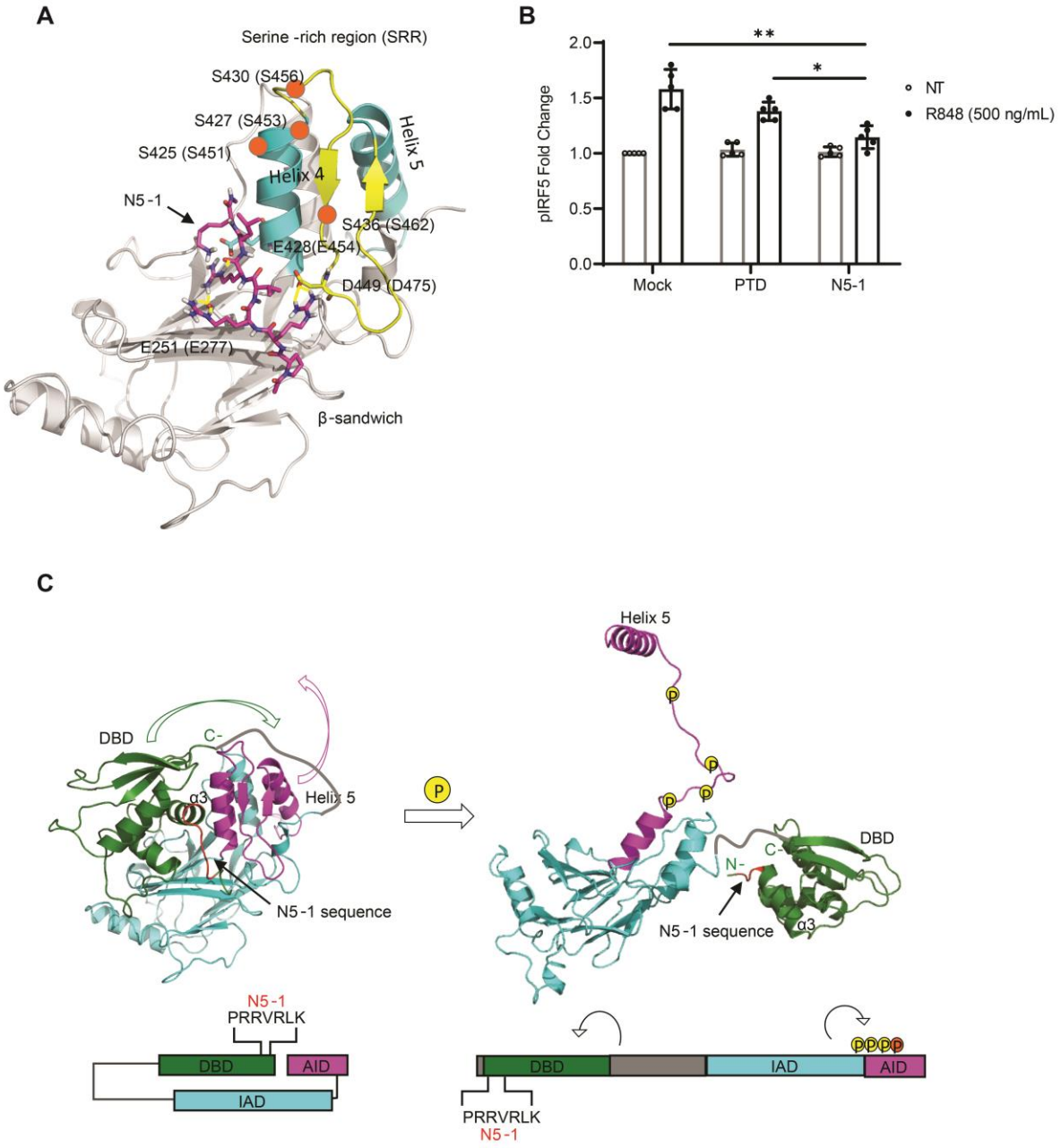

Fig. 3. N5-1 is predicted to bind to the C-terminal IAD of an inactive IRF5 monomer and inhibit phosphorylation of Ser462. (**A**) Schematic diagram of N5-1 (pink) binding to the C-terminal IAD of IRF5 from peptide docking using the Schrodinger suite (Suppl. Methods). N5-1 stabilizes the non-phosphorylated, inactive IRF5 monomer. Serine phosphorylation sites are shown by orange circles. (**B**) PBMCs were pre-incubated with 10 μM of inhibitor for 1 h and stimulated with R848. IRF5 phosphorylation at Ser462 (pIRF5) was detected by flow cytometry following gating on $CD14^+$ Mo. Fold-change in pIRF5 relative to unstimulated mock samples is shown; $n = 5$ independent healthy donors. Statistical significance was determined by one-way ANOVA. Error bars represent SD. *($p \leq 0.05$), **($p \leq 0.01$). (**C**) Based on the binding of N5-1 to full-length inactive IRF5, we propose that the DBD masks the IAD of IRF5 and the AID masks

the C-terminal phosphorylation sites, thus stabilizing a closed unphosphorylated conformation of the IRF5 monomer (left side). In this conformation, the DBD α3 helix, which contains all the conserved residues and is responsible for protein-DNA contacts, is shieded. Upon phosphorylation, the AID unfolds, which unmasks the C-terminal phosphorylation sites and frees helix 5 for dimerization (right side). The DBD will also be released from this folded, inactive position and exposed to DNA for binding. Colors correspond to the specified regions of IRF5 in the crystal structure (above) and the stick model (below). Green represents the DBD, blue the IAD, and purple the AID. The N5-1 sequence is shown in red in both models.

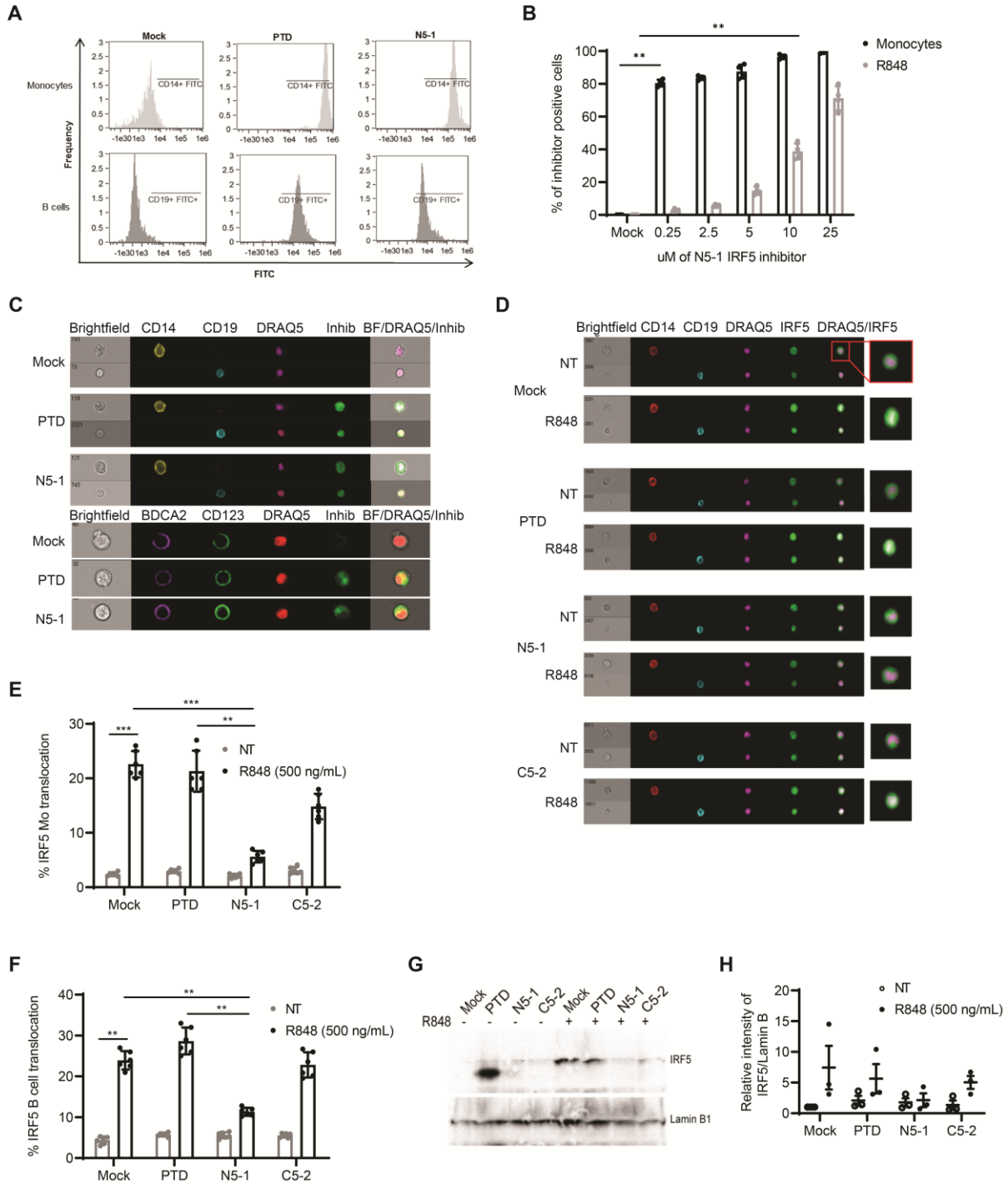

Fig. 4. IRF5 peptide inhibitors readily enter primary immune cells to inhibit R848-induced IRF5 nuclear translocation. (**A**) Representative flow cytometry histograms showing uptake of 10 μM FITC-conjugated PTD or N5-1 after incubation of human PBMC with inhibitor for 1 h. Inhibitor uptake defined as FITC-positive >10^4 in $CD14^+$ Mo (light gray) and 10^3 in $CD19^+$ B cells (dark gray). (**B**) Percent of total Mo and B cells positive for FITC-conjugated N5-1; *n* = 4 independent healthy donors. (**C**) Representative images of cellular uptake of 10 μM FITC-conjugated PTD or N5-1 in either Mo (top row), B cells (bottom row) or pDCs (bottom panel).

(**D**) Representative images of IRF5 cellular localization in Mo (CD14) and B cells (CD19) after pre-incubation of PBMC with 10 µM mock, PTD, N5-1, or C5-2 inhibitors followed by stimulation with 500 ng/mL R848 for 2 h. (**E** and **F**) Quantification of IRF5 nuclear translocation in Mo (**E**) and B cells (**F**) was done by imaging flow cytometry; $n = 6$ independent healthy donors. (**G**) Representative Western blot of nuclear extracts from primary human Mo following treatment with 2.5 µM of mock, PTD, N5-1, or C5-2 inhibitors and stimulation with 500 ng/mL R848 for 2 h. (**H**) Quantification of nuclear IRF5 from (**G**) relative to Lamin B1; $n = 3$ independent healthy donors. Representative data are from ≥3 independent experimental replicates. Statistical significance was determined by one-way ANOVA. Error bars represent SEM. **($p \leq 0.01$), ***($p \leq 0.001$).

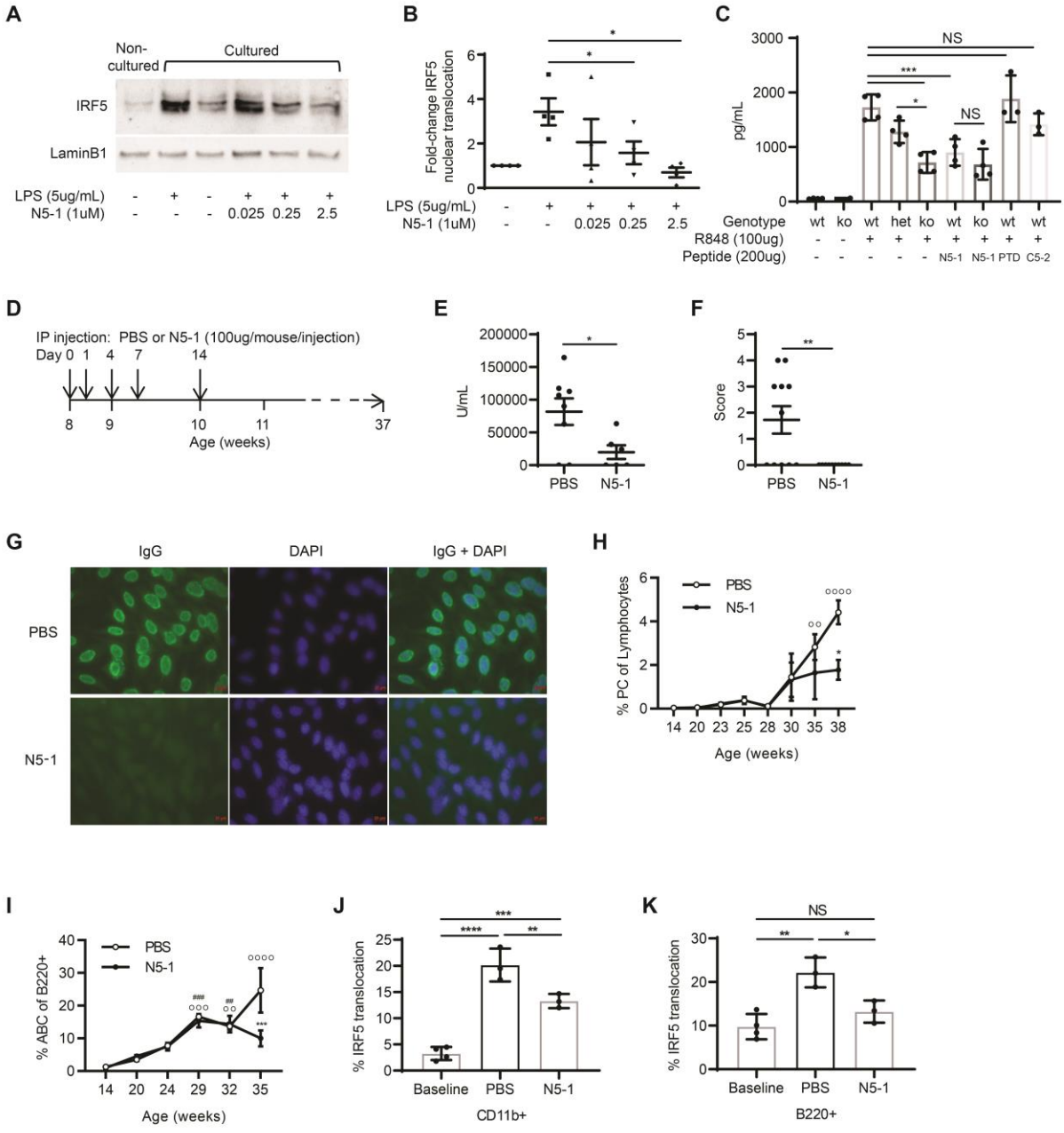

Fig. 5. N5-1 protects NZB/W mice from spontaneous lupus onset. (**A**) Representative Western blot of nuclear extracts from RAW264.7 macrophages pre-treated for 1 h with N5-1 followed by LPS for 2 h. Non-cultured cells, 0 h before pre-treatment; cultured cells, 3 h post-treatment. (**B**) Quantification of nuclear IRF5 in (**A**) relative to Lamin B1 from 3 independent replicates. Statistical significance by one-way ANOVA. (**C**) *In vivo* inhibition of IL6 secretion by N5-1 in wt (*Irf5*$^{+/+}$), het (*Irf5*$^{+/-}$) and ko (*Irf5*$^{-/-}$) mice. Sera harvested at 1.5 h post-R848; *n* = 3-4 mice/group. Statistical significance was by one-way ANOVA. (**D**) N5-1 dosing strategy for NZB/W F1 mice. (**E**) Anti-dsDNA Ig titers (1:500 serum dilution) at 20 weeks-old. (**F**) ANA immunofluorescence scoring from sera of *n* = 11 PBS- and *n* = 10 N5-1-treated mice. 0, negative signal; 4, strongest signal. Statistical significance determined by Mann-Whitney test. (**G**) Representative ANA images

from 27 week-old treated mice (20X objective x 10X eyepiece). (**H** and **I**) Percentage of circulating $IgD^{-}B220CD138^{+}$ PCs (PC; **H**) and $B220^{+}CD11c^{+}CD11b^{+}$ ABCs (**I**). n = 4 mice/time point. Statistical significance determined by two-way ANOVA and Bonferroni's multiple comparisons test (**H**) ($F(7,35)=10.27$, $p<0.0001$ age; $F(1,35)=4.125$, $p=0.049$ treatment; $F(7,35)=1.627$, $p=0.1603$ interaction). *($p=0.0133$ vs PBS, week 38; $^{oo}p<0.0081$ and $^{oooo}p<0.0001$ vs PBS, week 14). (**I**) $F(5,32)=20.63$, $p<0.0001$ age; $F(1,32)=4.402$, $p=0.0439$ treatment; $F(5,32)=4.146$, $p=0.0051$ interaction). ***$p=0.0001$ vs PBS, week 35; $^{oo}p=0.0033$, $^{ooo}p=0.0002$ and $^{oooo}p<0.0001$ vs PBS, week 14; $^{\#\#}p=0.0005$, $^{\#\#\#}p=0.0029$ vs N5-1, week 14). (**J** and **K**) Inhibition of Irf5 activation in cohort 2 (14-21 weeks-old) by N5-1; $CD11b^{+}$ Mo (**J**) and $B220^{+}$ (**K**) B cells. n = 4 mice/group. Statistical significance determined by one-way ANOVA. All values reported as mean ± SEM. *($p \leq 0.05$), **($p \leq 0.01$), ***($p \leq 0.001$), ****($p \leq 0.0001$).

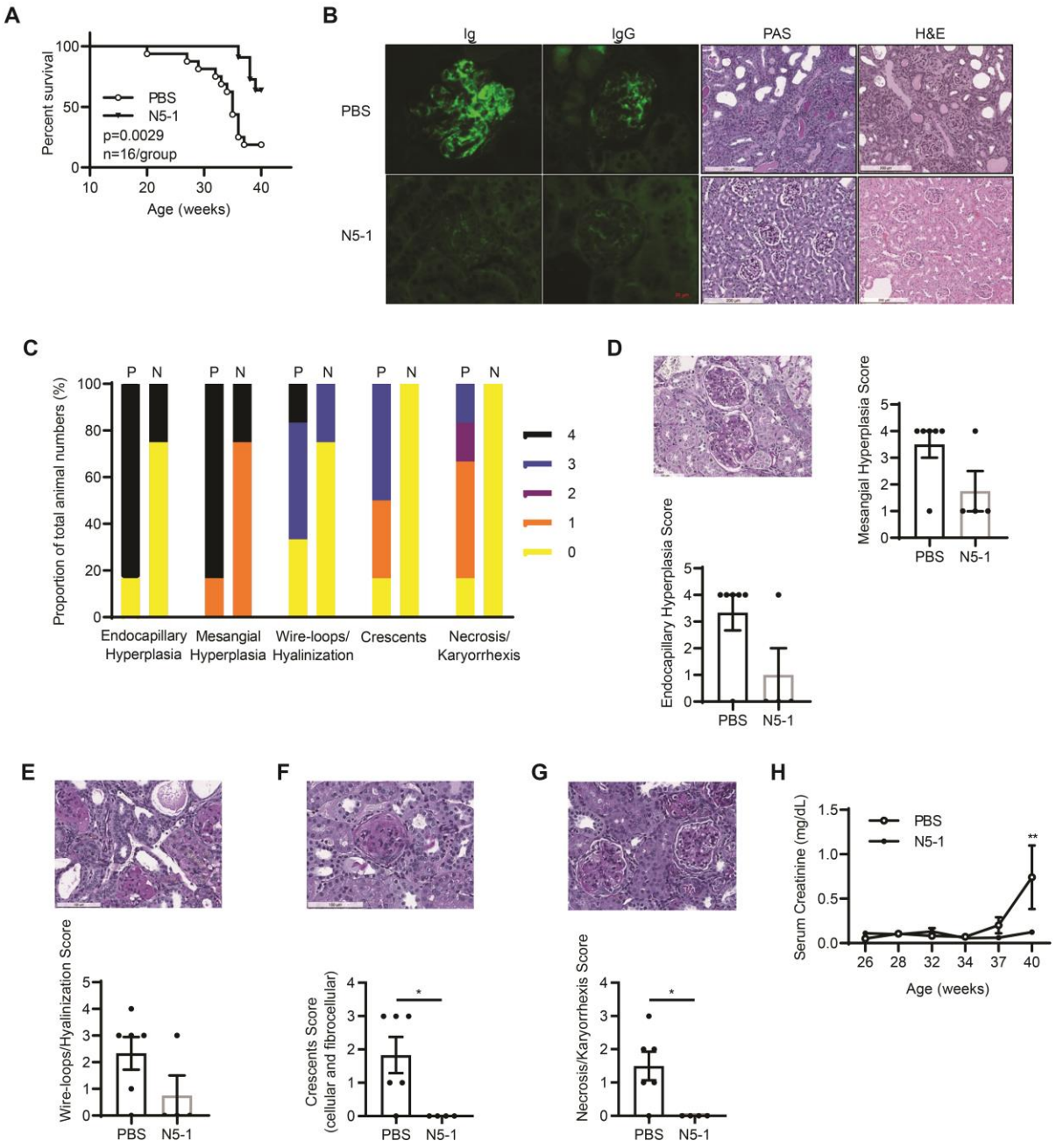

Fig. 6. N5-1 reduces kidney pathology and increases overall survival. (**A**) Kaplan-Meier survival curves. Differences determined by Gehan-Breslow-Wilcoxon test. *n* = 11 mice/group. (**B**) Representative microscopy images of renal sections; fluorescence deposition of Ig and IgG (40X magnification), periodic acid-Schiff (PAS) and haemotoxylin and eosin (H&E) staining (10X magnification). (**C**) Summarized scoring of renal inflammation and damage shown in (**D-G**) from *n* = 6 PBS-treated and *n* = 4 N5-1-treated mice. (**D-G**) Microscopy images of renal sections assessed by PAS staining (20X magnification) showing images of endocapillary and mesangial hyperplasia (**D**), wire-loops/hyalinization (**E**), crescents (**F**) and necrosis/karyorrhexis (**G**). Scoring of 100 glomeruli per case is shown. (**H**) Serum creatinine levels plotted over the course

of disease. n = 8 mice/group. Statistical significance was determined by Mann-Whitney test. *($p \leq 0.05$).

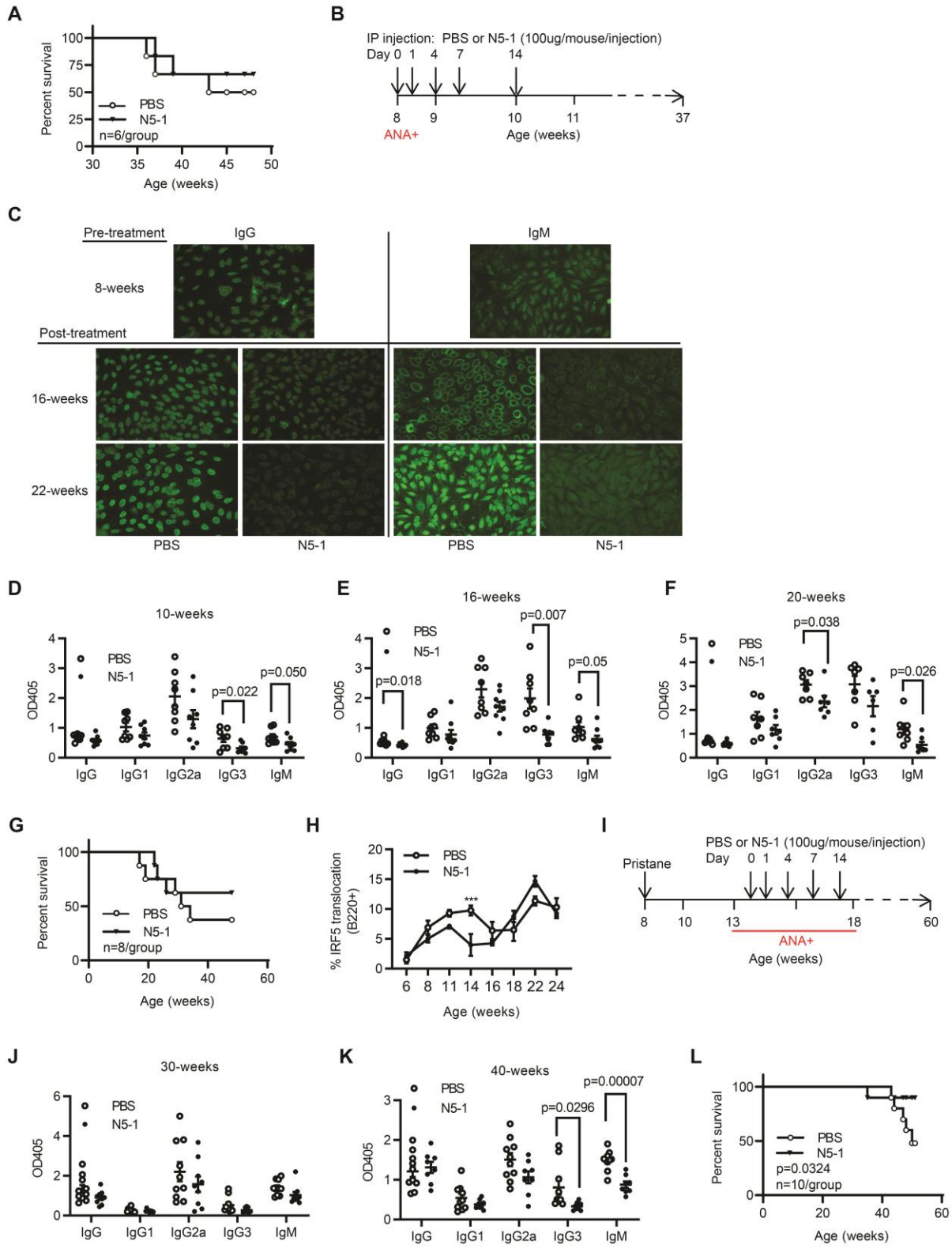

Fig. 7. Therapeutic efficacy of N5-1 in ANA-positive NZB/W F1, MRL/lpr and pristane-induced lupus mice. (**A**) Kaplan-Meier survival curves of NZB/W F1 mice treated at 27 weeks-

old. Differences determined by Gehan-Breslow-Wilcoxon test. *n* = 6 mice/group. (**B**) N5-1 dosing strategy for MRL/lpr mice. (**C**) Representative ANA images from 8-week-old pre-treated mice and 16- and 22-week-old treated mice (20X objective x 10X eyepiece). (**D-F**) Anti-dsDNA IgG isotype titers (1:500 serum dilution) were determined at the indicated ages. (**G**) Kaplan-Meier survival curves of MRL/lpr treated mice. Differences determined by Gehan-Breslow-Wilcoxon test. *n* = 8 mice/group. (**H**) Analysis of Irf5 nuclear translocation in $B220^{+}$ B cells from PBS- and N5-1-treated MRL/lpr mice. *n* = 8 mice/group. (**I**) N5-1 dosing strategy for pristane-injected mice. (**J** and **K**) Anti-dsDNA IgG isotype titers (1:500 serum dilution) were determined at the indicated ages. (**L**) Kaplan-Meier survival curves of pristane-induced Balb/c mice. Differences determined by Gehan-Breslow-Wilcoxon test. *n* = 10 mice/group. (**D-F, H, J, K**) Statistical significance was determined by Mann-Whitney test. ***($p \leq 0.0001$).

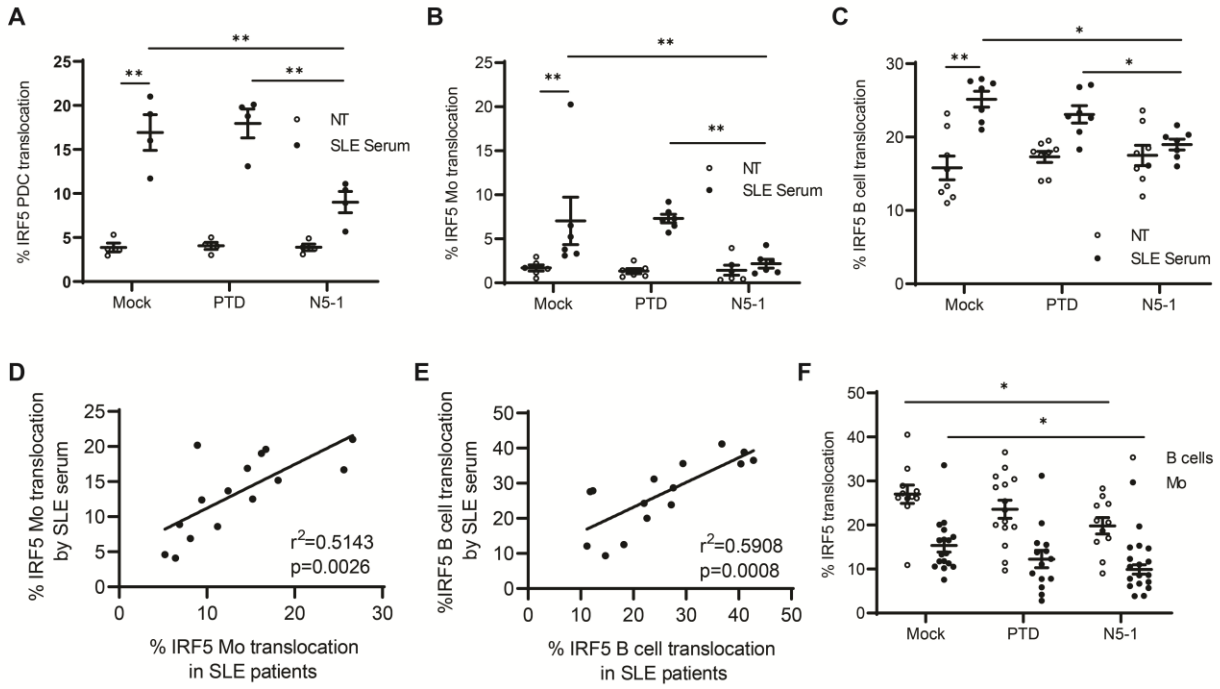

Fig. 8. N5-1 inhibits SLE serum-induced IRF5 activation and reverses IRF5 hyper-activation in SLE immune cells. (**A**) Healthy donor PBMC (n = 6) were pre-incubated with 10 μM inhibitor followed by stimulation with 2% SLE serum for 2 h. % IRF5 nuclear translocation is shown in pDCs (**A**), Mo (**B**) and B cells (**C**) from imaging flow cytometry. (**D** and **E**) Correlation between % IRF5 translocation in SLE serum-stimulated Mo (**D**) or B cells (**E**) and *in vivo* IRF5 activation in matched SLE Mo or B cells, respectively, by linear regression. (**F**) SLE PBMC were mock- or inhibitor-treated (10 μM) for 1 h and IRF5 activation quantified by imaging flow cytometry in Mo and B cells. % IRF5 nuclear translocation is shown. Differences between groups determined by two-way ANOVA with Bonferroni's multiple comparisons. Values reported as mean ± SEM. *($p \leq 0.05$), **($p \leq 0.01$).